

A feedback neural circuit for calibrating aversive memory strength

Takaaki Ozawa^{1,5}, Edgar A Ycu^{1,6}, Ashwani Kumar^{1,2,6}, Li-Feng Yeh^{1,3,6}, Touqeer Ahmed⁴, Jenny Koivumaa¹ & Joshua P Johansen^{1,3}

Aversive experiences powerfully regulate memory formation, and memory strength is proportional to the intensity of these experiences. Inhibition of the neural circuits that convey aversive signals when they are predicted by other sensory stimuli is hypothesized to set associative memory strength. However, the neural circuit mechanisms that produce this predictive inhibition to regulate memory formation are unknown. Here we show that predictive sensory cues recruit a descending feedback circuit from the central amygdala that activates a specific population of midbrain periaqueductal gray pain-modulatory neurons to control aversive memory strength. Optogenetic inhibition of this pathway disinhibited predicted aversive responses in lateral amygdala neurons, which store fear memories, resulting in the resetting of fear learning levels. These results reveal a control mechanism for calibrating learning signals to adaptively regulate the strength of behavioral learning. Dysregulation of this circuit could contribute to psychiatric disorders associated with heightened fear responsiveness.

Salient aversive or rewarding experiences trigger learning by activating neural ‘instructive’ pathways, which alter connectivity in brain regions responsible for storing memories^{1–4}. Over the course of learning, activation of these instructive signaling pathways by salient events is inhibited as other sensory features of the environment come to predict their occurrence. Predictive inhibition of instructive signaling is apparent across diverse learning circuits, including those involved in reward, fear, motor, sensory localization and vocal learning^{1,2,5–8}. This has typically been termed ‘prediction error’ coding, as salient events only activate these instructive circuits when they occur unexpectedly. Prediction error coding has been suggested to set the maximal strength of learning (the ‘learning asymptote’) proportionally to the strength of aversive or rewarding outcomes through inhibition of instructive signaling circuits as the outcome becomes expected^{9,10}. Prediction errors have been hypothesized to occur through long-range neural feedback pathways conveying predictive sensory information, which inhibit instructive signaling circuits^{1,2,5,6,11,12}. How neural circuits construct prediction error signaling, however, is not well understood, and whether these mechanisms control the strength of associative memories is unknown.

Here we examined these questions in an aversive-learning circuit responsible for fear-memory formation. During auditory fear (‘threat’¹³) conditioning, animals learn that an auditory stimulus (conditioned stimulus, CS) predicts the occurrence of an aversive outcome (unconditioned stimulus, US; typically a mild electric shock) and exhibit measurable behavioral and visceral fear responses to the auditory CS after learning^{5,14–18}. Activation of lateral amygdala (LA)

pyramidal neurons by aversive shocks produces synaptic strengthening of auditory inputs onto LA neurons and enhancement of auditory processing, resulting in fear memory storage^{16,19–21}. Aversive-coding LA and basal amygdala cells project to the central amygdala (CeA)²², which projects in turn to the periaqueductal gray (PAG) and other brain regions to produce defensive responses including freezing^{5,14–18}. Notably, fear-learning asymptotes are proportional to the intensity of the aversive experience, with higher shock intensities resulting in stronger fear memories^{23,24}. Aversive responses in LA neurons are encoded as prediction errors, as cells there respond more strongly to unpredicted aversive outcomes than to those outcomes predicted by auditory cues^{25,26}. This learning-dependent inhibition of aversive processing in LA neurons could provide a mechanism for setting learning asymptotes^{23,24}.

How aversive prediction errors are created by the fear circuit and whether they control fear memory strength is not well understood. Based on a previous conceptual model¹², we hypothesized that a specific CeA–PAG feedback circuit, distinct from the PAG freezing-response pathway, inhibits aversive processing before it reaches the LA. Supporting this idea, CeA neurons that project to the PAG increase their response to auditory CSs during fear learning^{27,28}, and the magnitude of auditory CS-evoked responses in amygdala neurons reflects the intensity of the aversive outcome²⁹. Furthermore, PAG neurons respond to auditory stimuli following learning, and projections from the ventrolateral PAG subregion (vIPAG) to the rostral ventromedial medulla (RVM) are part of a pain-inhibitory circuit that mitigates nociceptive processing in the spinal cord^{25,30–33}.

¹RIKEN Brain Science Institute, Laboratory for Neural Circuitry of Memory, Saitama, Japan. ²Sant Longowal Institute of Engineering and Technology (SLIET), Electrical and Instrumentation Engineering Department, Sangrur, India. ³Department of Life Sciences, Graduate School of Arts and Sciences, University of Tokyo, Tokyo, Japan. ⁴National University of Sciences and Technology, Atta-ur-Rahman School of Applied Biosciences, Islamabad, Pakistan. ⁵Present address: Department of Basic Neurosciences, University of Geneva, Geneva, Switzerland. ⁶These authors contributed equally to this work. Correspondence should be addressed to J.P.J. (jjohans@brain.riken.jp).

Received 29 July; accepted 6 October; published online 14 November 2016; doi:10.1038/nn.4439

Consistent with our hypothesis, we found that a vPAG-to-RVM pathway was activated by sensory predictive cues through CeA inputs to the PAG. Furthermore, this circuit inhibited aversive signaling and ultimately set prediction-error coding in LA neurons, thereby controlling behavioral learning asymptotes. These findings reveal an amygdala–PAG–brainstem descending feedback circuit for inhibiting expected aversive signals to set memory strength, suggesting a general circuit mechanism for prediction-error coding that could be used in many learning systems.

CeA-to-vPAG circuit regulates prediction error coding in LA neurons

To examine whether a CeA–vPAG pathway participates in setting prediction-error coding in LA neurons, we tested whether optogenetic inactivation of CeA axon terminals in vPAG reversed the reduction of aversive shock-evoked responses in LA neurons when the shock was predicted by the auditory CS. We focused our analysis on the LA because of its importance as a site of synaptic plasticity mediating fear-memory storage^{5,14,16–18} where prediction errors could directly regulate learning. We injected adeno-associated viral (AAV) vectors into CeA to express the light-activated inhibitory opsin Archaeorhodopsin-T (ArchT) in CeA cell bodies and axon terminals in PAG (Fig. 1a). We could then inhibit terminal release of the CeA inputs to the vPAG specifically during the CS–US period by delivering laser light into the vPAG^{34,35}. Using weak eyelid shocks, we found that behavioral learning asymptotes were achieved after one day of training at a specific shock intensity, as further training did not induce higher freezing levels unless the shock intensity was increased during overtraining (Supplementary Fig. 1). Having established this behavioral model, we then implanted stereotrodes into the LA and recorded single-unit spiking activity of LA neurons from well-trained animals during unpredicted and predicted shocks, as well as during predicted shocks concurrent with laser inactivation of CeA–vPAG terminals (Fig. 1a and Supplementary Fig. 2a). Previously, we had found prediction-error coding cells in LA²⁰, and we replicated that here, showing that 37 of 121 shock-responsive cells in LA exhibited stronger shock-evoked neural responses to unpredicted shocks compared to CS-predicted shocks. However, when CeA–vPAG terminals were inhibited, predicted-shock-evoked responses in LA prediction-error coding neurons were significantly enhanced (Fig. 1b–d and Supplementary Fig. 3a). This effect was not apparent in non-prediction-error coding LA cells (Supplementary Fig. 3b,c), suggesting that inactivation of the CeA–vPAG pathway does not generally disinhibit shock processing. Consistent with a previous report²⁵, prediction-error coding was apparent in cells with both high and low baseline firing rates, which have been defined in previous studies as comprising putative GABAergic and glutamatergic neurons, respectively (Supplementary Fig. 3d). Optical inhibition of the CeA–vPAG pathway alone had no effect on LA neural activity (Supplementary Fig. 3e), demonstrating that manipulations of this pathway alone do not alter baseline firing rates in LA neurons. We also found excitatory CS-evoked responses in 36% of LA neurons (65 of 180) after learning, but inactivation of the CeA–vPAG circuit had no effect on these responses (Fig. 1e). These results show that a CeA–vPAG circuit was necessary to inhibit aversive shock processing when the shock was predicted by auditory cues, as optogenetically inhibiting this pathway disinhibited predicted-shock-evoked responding in LA neurons (Fig. 1f).

Previous work suggested that the LA receives aversive US information from the PAG and that the dorsolateral and lateral PAG (dl/IPAG) may be the most important subregion for this process^{25,36,37}.

This aversive signaling pathway may function in parallel with a parabrachial-to-CeA pathway that also regulates fear learning^{38,39}, possibly by modulating plasticity occurring at LA–CeA synapses⁴⁰. Aversive prediction-error coding is also apparent in PAG cells, and the PAG receives a direct input from the spinal and trigeminal dorsal horn^{25,32,33}. Based on these data, we examined whether inhibition of the CeA–vPAG pathway disinhibited predicted-shock-responding in dl/IPAG prediction-error-coding cells as it does in LA neurons. We found that 33 of 108 shock-responsive cells in dl/IPAG were prediction-error coding. Consistent with what was observed in the LA, optogenetic inhibition of CeA–vPAG pathway disinhibited predicted-shock-evoked responses in these cells (Supplementary Fig. 4a–g). This shows that the effect of manipulating the CeA–vPAG pathway was evident even at very early stages of aversive processing, likely before these aversive signals reached the LA.

CeA-to-vPAG pathway sets behavioral learning asymptotes

Because shock-evoked activation of LA neurons is important for fear conditioning^{19–21} and this activation is reduced once shocks become predicted through learning²⁵, we hypothesized that the CeA–vPAG circuit may function to set behavioral learning asymptotes by inhibiting shock-evoked activation in the fear system. To test whether the CeA–vPAG circuit sets learning asymptotes, we trained animals to their learning asymptote using a behavioral model similar to that described above, and then optogenetically inactivated this pathway. Specifically, this behavioral assay utilized a 4-d fear-conditioning model in which animals were trained on days 1 and 3 and their tone-CS-evoked behavioral freezing responses were assayed after 1 or 2 d of training on days 2 (Test 1) and 4 (Test 2) (Supplementary Fig. 5a). Behavioral freezing levels after 1 d of training and after overtraining on day 3 were not different unless the shock intensity was increased. As a behavioral control, we confirmed that the single CS exposure on Test 1 did not induce any extinction in the absence of overtraining when measured at Test 2 (Supplementary Fig. 5b). Using this behavioral model, we next tested whether bilateral optogenetic inactivation of CeA–vPAG pathway during the CS–US period of overtraining ('Overlap' group) increased learning asymptotes when the shock intensity was held constant (Fig. 2a). We compared the effects of this manipulation in the Overlap experimental group to a control group of animals in which GFP, instead of ArchT, was expressed in CeA–vPAG terminals (GFP control) and to a second control group in which ArchT was expressed in CeA terminals but the inhibition occurred after, rather than during, the CS–US period ('Offset' group). While similar levels of freezing between tests 1 and 2 were seen in the two control groups, freezing was significantly increased after overtraining in the Overlap group even though the shock intensity was not increased (Fig. 2b). To determine whether this effect was specific to CeA terminals in vPAG we performed the same experiment in dl/IPAG (where CeA axons were also evident; Fig. 1a). Under these conditions, we saw no effect of terminal inhibition, demonstrating specificity of function for CeA neuronal projections to distinct PAG subregions (Supplementary Fig. 6a,b). To determine whether this learning enhancement was specific to asymptotic learning and not due to general enhancement of fear learning, we examined the effect of CeA–vPAG terminal inhibition on nonasymptotic learning induced by a single CS–US pairing, in which the shock US was not predicted at all. In this case, inhibition of the CeA–vPAG pathway had no effect on conditioning (Supplementary Fig. 6c). Together, these data demonstrate that a CeA–vPAG circuit was necessary to set stable behavioral learning asymptotes, as inactivation of this pathway during asymptotic learning increased fear memory strength.

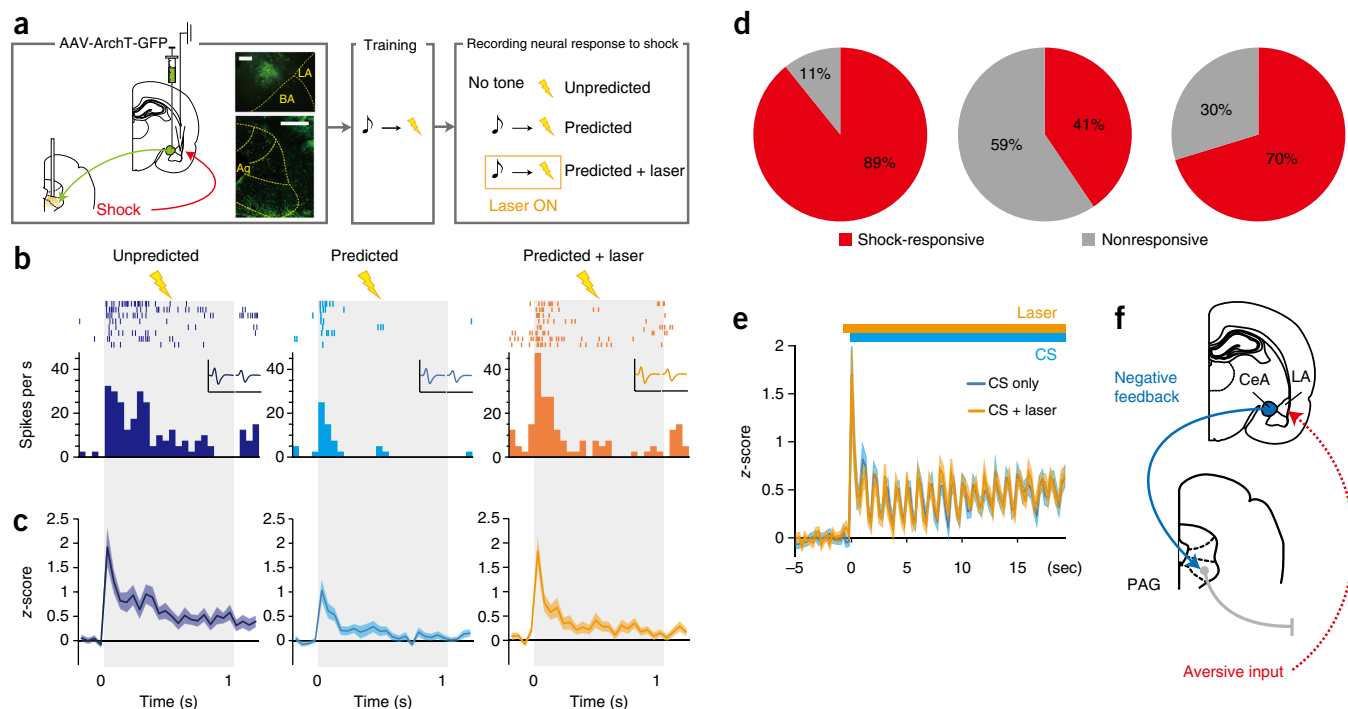


Figure 1 Prediction-error signaling in LA neurons re-emerges with optogenetic inhibition of CeA inputs to vIPAG. **(a)** Schematic of experimental paradigm. Left, virus injection in CeA, optical fiber implant and light delivery in vIPAG, and single-unit recordings in LA. Middle, training via tone–shock pairings. Right, electrophysiological recording protocol. Scale bars indicate 200 μm for CeA and 1 mm for PAG. **(b)** Perievent time histograms (PETH, 50-ms bins) and raster plots showing an example prediction-error-coding cell in LA exhibiting disinhibition of shock-evoked responding when CeA–vIPAG pathway is optically inhibited. Insets show average waveforms on two stereotrode channels during the different trial types (complete scale on y-axis is 0.2 mV and 1 ms on x-axis). Shock periods for each trial type are shown in gray area (1 s). **(c)** Same as **b**, except that PETHs plot the z-score averaged response (y-axis) of all prediction-error-coding cells recorded in LA ($n = 37$ of 121 total shock-responsive cells from 3 animals). See **Supplementary Figure 3a** for population response analysis. **(d)** Circle plots showing proportion of prediction-error-coding cells that were significantly shock-responsive or nonresponsive in unpredicted, predicted and predicted + laser conditions aligned to the PETH in **b** and **c**. χ^2 test with Bonferroni correction ($\alpha = 0.0166$) revealed a significantly higher proportion of shock-responsive cells in the unpredicted vs. predicted conditions ($\chi^2_{(1)} = 19.212$, $P = 0.0001$) and Predicted + laser vs. Predicted conditions ($\chi^2_{(1)} = 6.618$, $P = 0.0001$). **(e)** PETH showing population averaged firing rates (y-axis) of all CS-responsive cells ($n = 65$ of 180 total cells) during the auditory-CS period (20 s starting at 0, x-axis) without (blue trace) or with (orange trace) light-induced inhibition of the CeA–vIPAG pathway. A two-tailed paired t -test revealed that inhibition of this pathway did not change excitatory CS-evoked response in LA ($t_{(64)} = 0.0579$, $P = 0.9596$). **(f)** Working model showing the CS-responsive negative-feedback pathway from CeA–vIPAG (blue) and the aversive-US pathway (red) as well as undefined circuit(s) (gray). See **Supplementary Figure 3**. In **c** and **e**, data are presented as mean \pm s.e.m.

LA prediction errors control learning asymptotes

Shock-evoked activation of LA neurons is critical for fear learning^{19,20} and our findings here show that optogenetic inactivation of the CeA–vIPAG pathway produced disinhibition of predicted-shock-evoked responses in LA neurons. Based on these results we hypothesized that the increase in behavioral learning asymptotes induced by optogenetic CeA–vIPAG inhibition resulted from a disinhibition of shock-evoked responding in LA neurons. To test this, we infused muscimol, a GABA_A receptor agonist, or its vehicle (PBS) into the LA to silence neural activity there before overtraining on day 3 when CeA–vIPAG was optogenetically inactivated during the CS + US period (**Fig. 2c**). We found that CeA–vIPAG inhibition increased learning asymptotes in the PBS control group (**Fig. 2d**), replicating our results above (**Fig. 2b**). However, inhibition of CeA–vIPAG terminals did not enhance learning when LA neurons were inhibited by muscimol during overtraining (Muscimol group; **Fig. 2d**). Notably, infusion of muscimol into LA during overtraining did not affect learning asymptotes on its own (**Supplementary Fig. 6d**). These results demonstrate that neural activity in LA was necessary for the increase in learning asymptotes produced by optogenetic inhibition of the CeA–vIPAG pathway during overtraining. To further investigate the functional importance of prediction-error coding in LA, we optogenetically activated

principal neurons in LA to mimic the disinhibition of prediction-error coding seen during overtraining with terminal inactivation of the CeA–vIPAG pathway. To do this we expressed the blue-light-activated channelrhodopsin-2 (ChR2) in LA pyramidal cells^{19,20} and delivered laser light into LA during the shock-US period of overtraining (**Fig. 2e**). Additive activation of LA pyramidal neurons in this Overlap group during the shock period of overtraining produced an increase in CS-evoked freezing between Test 1 and Test 2 (**Fig. 2f**). By contrast, freezing levels were not changed in the eYFP and Offset control groups. Together, these data suggest that the CeA–vIPAG pathway regulated behavioral fear learning asymptotes by disinhibiting predicted-shock-evoked responding in LA neurons and that prediction-error coding in these cells was causally involved in setting learning asymptotes.

Auditory predictive cues activate vIPAG neurons through the CeA–PAG pathway

The above results show that the CeA–vIPAG pathway functions as a negative feedback circuit to set prediction-error coding in LA neurons and behavioral learning asymptotes. However, it is not clear how terminal inactivation of this pathway regulates vIPAG neural coding to produce this effect. Because it is known that many PAG-projecting

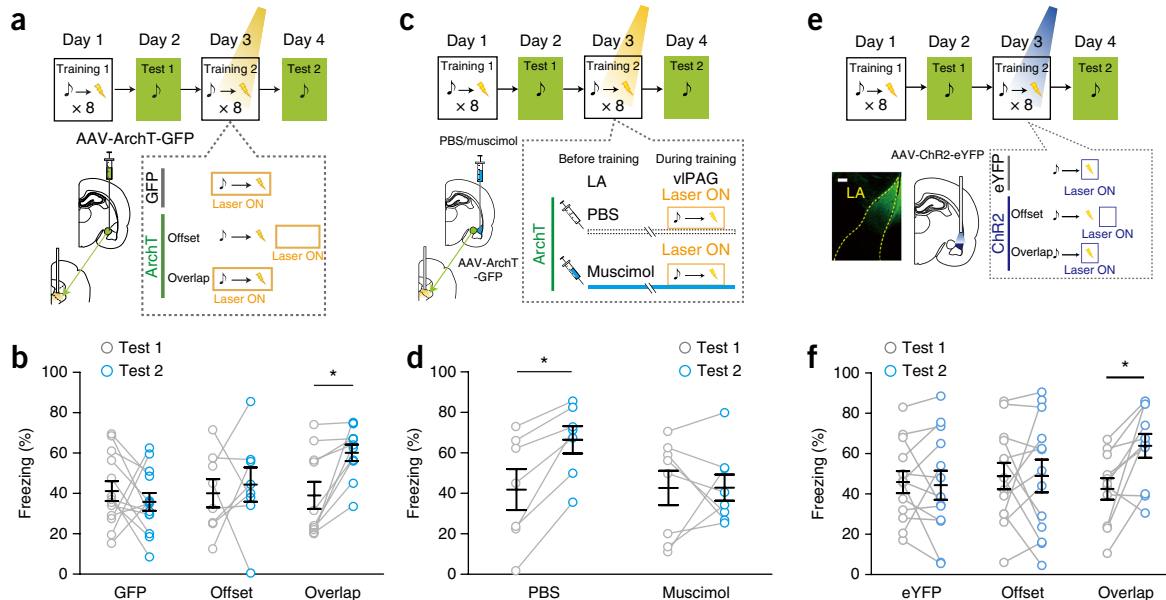


Figure 2 CeA–vIPAG pathway controls learning asymptotes by regulating prediction-error coding in LA. **(a)** Schematic of experimental model showing optogenetic manipulation of CeA–vIPAG pathway specifically during overtraining and learning asymptote. **(b)** Inhibition of CeA–vIPAG pathway during auditory-CS and shock-US periods of overtraining (Overlap group, $n = 10$) increased freezing levels (y-axis) in Test 2 compared with Test 1 (two-way repeated measures ANOVA, $F_{(2,28)} = 3.356$, $P = 0.0494$; Bonferroni *post hoc* test, $*P = 0.012$), which did not occur in the GFP ($n = 13$, $P = 0.409$) or Offset ($n = 8$, $P = 0.646$) control groups. **(c)** Schematic of experimental model showing a procedure similar to that used in **a**, in which the CeA–vIPAG pathway is optogenetically inhibited, except that muscimol or vehicle (PBS) was administered to LA before optogenetic inhibition. **(d)** Blocking neural activity in LA neurons with muscimol ($n = 8$) during overtraining abolished the enhancing effect of CeA–vIPAG inhibition on freezing responses (y-axis) from Test 1 to Test 2 (two-way repeated measures ANOVA, $F_{(1,13)} = 5.614$, $P = 0.0340$; Bonferroni *post hoc* test, $P = 0.992$), which is apparent in the PBS-treated control group ($n = 7$; $*P = 0.007$). **(e)** Experimental design using ChR2 expression to stimulate LA pyramidal neurons during overtraining (scale bar, 200 μm). **(f)** Stimulating LA pyramidal neurons during the shock-US period of overtraining increased freezing responses from Test 1 to Test 2 in the Overlap group ($n = 11$; two-way repeated measures ANOVA, $F_{(2,34)} = 3.611$, $P = 0.0378$; Bonferroni *post hoc* test, $*P = 0.005$), but not in the eYFP or Offset groups ($n = 13$, $P = 0.764$ and $n = 13$, $P = 0.962$ respectively). In **b**, **d** and **f**, data are presented as mean \pm s.e.m.

CeA cells, as well as PAG neurons themselves, are activated by predictive CS after fear conditioning^{25,27,28}, we tested the hypothesis that inactivation of this pathway would reduce CS processing in vIPAG neurons. We first used trans-synaptic rabies virus tracing (Online Methods) from vIPAG neurons to show that CeA neurons provide synaptic input to vIPAG (**Supplementary Fig. 7a**), consistent with previous anatomical results^{32,33,41}. We then recorded auditory-evoked responses from single vIPAG neurons after fear conditioning (**Fig. 3a**) and found excitatory auditory-CS-evoked responses in 53% of vIPAG neurons (79 of 147; **Fig. 3b,c**) and both short-latency and longer-latency ramping responses were apparent. This likely occurred through a disinhibitory process, as PAG-projecting CeA neurons are known to be GABAergic and disinhibit vIPAG projection neurons⁴¹. We next examined the effect of optogenetic inhibition of the CeA–vIPAG pathway on auditory evoked responses and found that these responses were decreased in CS-responsive vIPAG neurons when the CeA–vIPAG pathway was inactivated (**Fig. 3c,d**). This effect was only apparent in the longer-latency tonic component of the auditory-evoked response in these cells. We confirmed that laser illumination itself did not change the spontaneous firing rate of vIPAG neurons (**Supplementary Fig. 7b**), demonstrating that the optogenetic manipulation of the CeA–PAG projection did not induce suppression or excitation of vIPAG cell activity on its own. Finally, we found that this manipulation had no effect on auditory evoked responses in dl/vIPAG cells (**Supplementary Fig. 7c,d**). Thus, vIPAG neurons were activated by auditory predictive cues, and this activation was partially dependent on inputs from the CeA.

In addition to participating in prediction-error coding, vIPAG neural activity is also important in producing behavioral freezing responses^{32,33}, and these functions may be dissociable at the level of the vIPAG^{31,42}. One explanation for this could be that separate populations of neurons exist within vIPAG, one producing freezing responses and another providing auditory-CS-evoked feedback on the US-processing circuit. To test this explanation, we examined whether separate populations of cells were active during behavioral freezing responses and whether these cells overlapped with the auditory-CS-responsive neurons described above. Notably, we found separate populations of neurons that responded during behavioral freezing or to auditory CSs, respectively (**Fig. 3e–h**). In addition, a third population responded to both freezing and auditory stimuli. These data show that within vIPAG, partially distinct populations of neurons responded during behavioral freezing and auditory predictive cues.

Sensory cues activate specific vIPAG neurons through the CeA–PAG pathway to set learning strength

We next examined how the CeA–vIPAG pathway and auditory-evoked responding in vIPAG cells regulates behavioral learning asymptotes. Because vIPAG projections to RVM produce anti-nociception and because these brain regions are important for fear-conditioned analgesia^{12,30,31}, we hypothesized that CeA–vIPAG pathway recruits RVM-projecting vIPAG cells to control behavioral learning asymptotes. To test this hypothesis we examined whether RVM-projecting vIPAG neurons were activated by auditory CSs and whether this

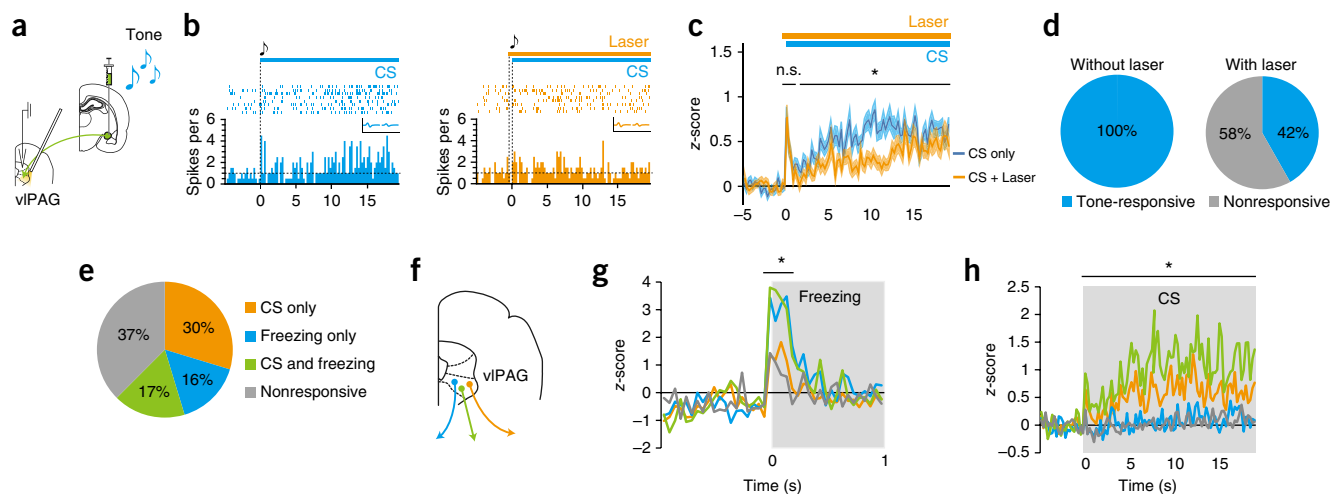


Figure 3 Excitatory auditory-cue processing is reduced in vIPAG neurons with optical inhibition of the CeA–vIPAG pathway. **(a)** Schematic of experimental model showing virus injection in CeA, and optical fiber implant and light delivery combined with single-unit recordings in vIPAG. **(b)** PETH (bin = 250 ms) and perievent raster plots showing auditory-CS (presentation time denoted by blue bar) responses in an example vIPAG cell without (left, blue panel) and with (right, orange panel) laser inhibition of CeA–vIPAG pathway. Insets show average waveforms on two stereotrode channels during auditory-CS period during the different trial types (complete scale on y-axis is 0.2 mV and 1 ms on x-axis). **(c)** Similar to **b**, but PETH (bin = 250 ms) shows population-averaged (y-axis) responses to auditory CS without (blue traces) and with (orange traces) laser inhibition of CeA–vIPAG pathway in vIPAG CS-responsive neurons ($n = 79$ of 147 total cells from 3 animals were CS-responsive). A two-tailed paired t -test revealed a significant reduction in later tonic auditory responses with terminal inhibition (after 1 s, $t_{(78)} = 6.786$, $*P = 0.0001$) but this manipulation did not affect the initial phasic auditory response (0–1 s, $t_{(78)} = 0.845$, $P = 0.401$). Data are presented as mean \pm s.e.m.; n.s., not significant. **(d)** Circle plots showing the proportion of vIPAG cells that were significantly auditory-CS-responsive or nonresponsive with and without laser inactivation of the CeA–vIPAG pathway. χ^2 test revealed a significantly higher proportion of auditory-CS-responsive cells in the Without laser vs. With laser conditions ($\chi^2_{(1)} = 24.22$, $P = 0.0001$). **(e)** Circle plot showing vIPAG cells sorted according to their auditory and freezing responsiveness. **(f)** Interpretative schematic showing different populations of vIPAG cells for auditory responding, freezing or both (colors match classification in **e**). **(g, h)** PETH (bin = 50 ms) showing population-averaged (y-axis) excitatory responses during **(g)** behavioral freezing onset (freezing onset at time 0) and **(h)** in response to auditory CS in auditory CS, freezing, auditory CS + freezing responsive and nonresponsive cell populations. Gray areas represent time periods of freezing onset or CS presentation used in analyses. In **g**, a one-way ANOVA revealed that freezing related excitatory responses (–50 to 350 ms around freezing onset) were significantly higher ($F_{(3,60)} = 8.735$, $P = 0.0001$) in the Freezing-only ($*P = 0.03$, vs. CS only; $*P = 0.003$, vs. nonresponsive cells by Bonferroni *post hoc* test) and CS + freezing cell populations compared to CS-only and nonresponsive cell populations (Bonferroni *post hoc* test $*P = 0.01$ for CS + freezing vs. CS-only cells, $*P = 0.001$ for CS + freezing vs. nonresponsive cells). In **h**, auditory-CS-evoked responses were significantly higher in CS and CS + freezing cell populations compared with auditory responding in freezing-only or nonresponsive cell populations ($F_{(3,60)} = 13.64$, $P = 0.0001$; Bonferroni *post hoc* test revealed $*P = 0.034$ for CS-only only vs. Freezing-only cells, $*P = 0.0001$ for CS-only vs. nonresponsive cells, $*P = 0.0001$ for CS + freezing vs. Freezing-only cells, $*P = 0.0001$ for CS + freezing vs. nonresponsive cells). Data are presented as mean \pm s.e.m.

activation was dependent on CeA inputs to vIPAG. To do this we injected a retrograde tracer into the RVM to label RVM-projecting cells in vIPAG (**Fig. 4a**). We then presented auditory CSs (or unpaired auditory stimuli or box exposure as control conditions) after learning to these animals and examined c-Fos immunoreactivity (using Fos-IR, a marker of activated cells) in RVM-projecting vIPAG neurons (**Fig. 4b**) to determine whether fear-inducing auditory cues activated this cell population. We found that Fos-IR in RVM-projecting vIPAG cells was increased in response to fearful auditory cues compared with control conditions (**Fig. 4b**), demonstrating that this vIPAG cell population was activated by predictive auditory cues. We then performed the same experiment with terminal inactivation of CeA inputs to vIPAG during the tone CS (**Fig. 4c**) and found that this manipulation reduced the auditory-evoked increase in Fos-IR in RVM-projecting cells compared with control animals (**Fig. 4d**). These data demonstrate that fear-inducing auditory cues activate RVM-projecting vIPAG cells and that, consistent with physiological data on unidentified vIPAG cells, inactivation of the CeA–vIPAG pathway reduces this activation.

Finally, we examined the functional role of this vIPAG cell population during the predictive-cue period of asymptotic fear learning. Specifically we asked whether inhibiting the activity of RVM-projecting vIPAG neurons during the CS–US period of overtraining increased

learning asymptotes like increasing shock intensity or inactivation of CeA inputs to vIPAG. To test this, we injected a retrograde canine adenovirus expressing Cre-recombinase (CAV2-Cre)⁴³ into the RVM followed by a Cre-dependent ArchT virus (AAV-FLEX-ArchT-GFP) into the vIPAG, allowing for optical inhibition of RVM-projecting vIPAG cells during the CS–US period of overtraining (**Fig. 4e**). This produced an increase in behavioral learning asymptotes compared with animals that received optical inhibition after the CS–US period (‘Offset’ controls; **Fig. 4f**). This same manipulation had no effect when animals were trained using single CS–US pairing (**Supplementary Fig. 7e**), demonstrating that laser inhibition of these cells did not enhance learning under conditions in which the CS did not predict the shock. Notably, inactivation of this pathway had no effect on behavioral freezing responses (**Fig. 4g, h**). To identify molecular markers of these cells, we then used immunohistochemistry combined with retrograde tracing and found that RVM-projecting vIPAG neurons were mostly glutamatergic, though a small population were GABAergic (**Supplementary Fig. 8a, b**). Together, these data show that fear-inducing auditory cues activate a vIPAG–RVM pain-modulatory circuit that controls learning asymptotes (but not freezing responses), suggesting that fear-learning asymptotes are regulated by auditory-cue-induced activation of a vIPAG–brainstem pain-modulatory circuit.

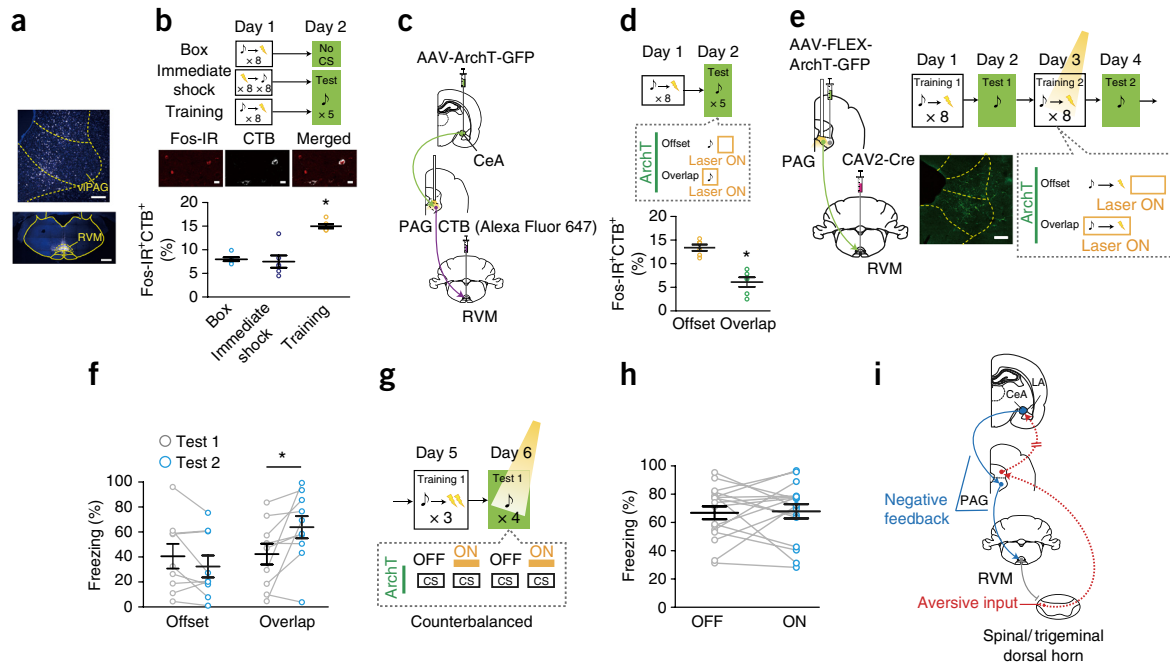


Figure 4 Auditory predictive cues recruit a CeA–vIPAG–RVM pathway to set behavioral learning asymptotes. **(a)** Retrograde cholera toxin B (CTB) tracer injections into RVM (bottom image shows injection site; scale bar, 200 μ m) produces robust cell-body labeling in vIPAG (top; scale bar, 1 mm). **(b)** Auditory CSs increase Fos-IR in RVM projecting vIPAG neurons. Top, schematic of experimental paradigm showing experimental (CS–shock US training followed by CS alone on day 2) and control (CS–US pairings, but exposure only to the conditioning box, or unpaired immediate shock) conditions ($n = 6$ for each). CTB injections were given before training and tissue was collected after the day 2 test, followed by Fos-IR and retrograde label quantification. Middle, example of Fos-IR- and CTB-labeled cells. Scale bar, 10 μ m. Bottom, quantification of percentage of colabeled Fos-IR+CTB+ cells (y -axis) in the three conditions. A one-way ANOVA followed by Bonferroni *post hoc* test revealed that a significantly higher percentage of cells in the training group were colabeled ($F_{(2,15)} = 25.94$, $P = 0.0001$) compared with cells from immediate shock ($*P = 0.001$) and box ($*P = 0.001$) control groups. **(c)** Schematic of CTB labeling and terminal manipulation approach for testing whether CeA–vIPAG inactivation reduced fearful auditory-induced increases in Fos-IR in RVM-projecting vIPAG cells. **(d)** Top, schematic of experimental model, as in **b** except that CeA inputs to vIPAG were inactivated overlapping or offset from the CS–US period during the day 2 test, followed by Fos-IR quantification. Bottom, quantification of Fos-IR+CTB+ colabeling, as in **b**. A two-tailed unpaired t -test revealed a significantly reduced Fos-IR+CTB+ colabeling in the Overlap group compared with the Offset group ($t_{(10)} = 7.733$, $*P = 0.0001$). **(e)** Schematic of methodology (left) and behavioral model (right) for specific optogenetic manipulation of RVM-projecting vIPAG neurons during overtraining. Image is a cross-section of PAG, showing expression of a Cre-dependent ArchT in RVM-projecting vIPAG cells. Scale bar, 200 μ m. **(f)** Inhibition of RVM-projecting vIPAG cells during auditory-CS–shock-US period of overtraining (Overlap group, $n = 10$) increased freezing levels (y -axis) from Test 1 compared with Test 2 (two-way repeated measures ANOVA, $F_{(1,17)} = 8.902$, $P = 0.008$; Bonferroni *post hoc* test, $*P = 0.023$) but not in the Offset ($n = 9$) control group ($P = 0.894$). **(g)** Schematic showing model for testing whether inactivation of RVM-projecting vIPAG neurons affected behavioral-CS-evoked freezing responses. **(h)** Freezing responses were not different when RVM-projecting vIPAG neurons were inhibited (ON) compared with light off periods (two-tailed paired t -test, $t_{(18)} = 0.2717$, $P = 0.789$). **(i)** Working model showing the CeA–vIPAG–RVM descending feedback pathway (blue) and the putative aversive US pathway (red). In **b**, **d**, **f** and **h**, data are presented as mean \pm s.e.m.

DISCUSSION

In a variety of neural systems, the ability of salient experiences to activate instructive signals is negatively regulated by learning^{1,2,5–8}. Here we demonstrated a distributed neural circuit mechanism for this process in the fear-learning system (**Fig. 4i**). We found that a feedback pathway from the CeA to the vIPAG was necessary for auditory predictive CSs to activate a specific population of brainstem-projecting vIPAG neurons. This pathway was also necessary to inhibit predicted aversive responding in LA neurons, as inactivation of the CeA–vIPAG terminals disinhibited predicted-shock-responding in LA cells. This effect was also apparent at early stages of aversive processing in the dl/IPAG, which receives direct input from the spinal cord and trigeminal dorsal horn. Furthermore, the CeA–vIPAG pathway and the vIPAG neurons that project to the RVM set adaptive fear-learning asymptotes, as optogenetic disruption of CeA inputs to vIPAG or of RVM projecting vIPAG neurons resulted in increased fear-learning levels. The enhancement of learning asymptotes by optogenetic inhibition of the CeA–vIPAG pathway was dependent on activation of LA neurons

and was reproducible by artificial induction of prediction-error signaling in LA pyramidal cells, directly linking prediction-error coding in LA to setting behavioral learning asymptotes. Together, these results elucidate a specific neural feedback pathway that is activated by sensory predictive cues and modulates aversive signaling, likely at very early stages of aversive sensory processing, to set prediction-error coding in an identified memory storage area and control the strength of fear memories.

Because a recent report examining terminal inhibition in reduced preparations found paradoxical enhancement of terminal release by Arch activation³⁴, our use of ArchT terminal silencing for many experiments is an experimental choice worthy of consideration. We used ArchT because it provided optimal terminal expression and has been shown to inhibit neurotransmitter release^{34,35}. The enhancement in terminal release reported in the previous study was only apparent after long-duration constant illumination. We selected short-duration stimulation protocols (all < 25 s), which Mahn *et al.*³⁴ suggest does not increase spontaneous neurotransmitter release and which we found

did not increase the baseline activity of vIPAG neurons. Another possible concern is that the illumination alone in the vIPAG nonspecifically affected vIPAG neural processing and/or compromised animals' ability to process auditory CS or shock US information. We think this is unlikely, because illuminating vIPAG in ArchT-treated animals had no effect on baseline firing rates in vIPAG neurons but did reduce auditory-CS-evoked responses. Furthermore, laser inhibition of the CeA–PAG pathway did not impair single-trial learning, had no effect on auditory-evoked responses in dl/IPAG or LA, and only enhanced US responses in prediction-error coding cells but not in other US-responsive cells.

A notable aspect of our results is the demonstration that predictive feedback circuits could modulate aversive sensory signals at early stages of processing to set prediction-error coding in the fear system. The PAG–RVM pathway is part of an opiate- and stress-responsive pain-modulatory circuit that can inhibit processing of noxious stimuli at the level of the spinal and trigeminal dorsal horn^{3,12,30,31}. This circuit can gate distinct aspects of somatosensory and nociceptive processing at the level of the dorsal horn⁴⁴, providing a potential explanation for why prediction-error coding but not all shock-evoked sensory signals is specifically disrupted when the CeA–vIPAG pathway is inhibited. Endogenous opioids in the PAG are important for producing fear-conditioned analgesia and blocking^{12,30,31,42}, a behavioral phenomenon that is thought to use prediction-error coding to reduce redundant sensory-outcome associations. Our results pinpoint a circuit mechanism for prediction-error coding that could be used to control these other processes, in addition to regulating learning asymptotes, through recruitment of this CeA–vIPAG–RVM pathway. However, there are many kinds of aversive experiences (some of which are non-nociceptive) and there is evidence that this type of fear-learning-induced negative feedback can modulate non-nociceptive forms of aversive learning as well⁴⁵. It is therefore likely that multiple levels of feedback occur at different stages of the aversive system to regulate a broad range of aversive experiences. While our results implicate the vIPAG cells that project to the RVM in setting learning asymptotes, these same vIPAG cells (or a parallel feedback circuit) could inhibit aversive processing in other brain regions, conveying different types of aversive signals.

Many learning systems utilize some form of prediction-error coding to regulate learning, but the feedback mechanisms for this process are unclear^{1,2,5–7}. One possibility is that different learning systems share similar circuit mechanisms for constructing prediction errors. In the ventral tegmental area (VTA) dopamine system and the cerebellar eyeblink circuit, GABAergic mechanisms^{6,46} have been identified that locally modulate prediction-error coding. In the dopamine system, however, other findings suggest that prediction errors are already present in some form before they reach the VTA⁴⁷. This indicates that reward prediction errors are partially encoded before they reach the VTA, possibly through negative feedback occurring at early stages of reward processing, and further refined there by local GABAergic networks and extrinsic inputs. Together with the data presented here, this suggests that predictive negative feedback occurring at both early and later stages of salient stimulus processing could represent a general feature of instructive prediction-error-coding circuits.

These results also have important implications for understanding PAG function. It is well established that different PAG subregions generate distinct types of innate and learned defensive responses, including behavioral freezing^{32,33,48}. In previous work we reported that the PAG is important not only for producing previously learned defensive responses but also for relaying aversive signals to the LA to trigger fear conditioning, possibly through the dl/IPAG^{25,36,37}.

Our results here demonstrate that a specific population of vIPAG neurons produced predictive feedback, but not freezing, and that these cells are mainly glutamatergic. In addition, we show that CeA inputs to vIPAG, but not dl/IPAG, regulate learning asymptotes. Furthermore, the effects of feedback-circuit manipulations on aversive-shock processing are apparent in dl/IPAG prediction-error coding cells. In contrast to the vIPAG feedback pathway we identified, a recent study⁴¹ found a separate population of glutamatergic vIPAG neurons that projects to a medullary motor control region and produces freezing behaviors. Together, our results and this previous work suggest that cell-type and compartmental specificity are important organizational features of PAG for producing multiple learning and defensive behavioral response functions.

A defining feature of anxiety disorders such as post-traumatic stress disorder (PTSD) is exaggerated, difficult-to-extinguish fear memories, and the prevalence of PTSD increases with repeated trauma exposure⁴⁹. Our results show that disruption of this circuit, which regulates fear-learning asymptotes, leads to potentiated fear learning over multiple exposures to aversive stimuli. Interestingly, aversive prediction errors have also been reported in human PAG using functional imaging⁵⁰. It is possible that dysregulation of similar feedback circuits in humans could lead to heightened and persistent fear memories in individuals predisposed to anxiety disorders. This provides a testable framework for understanding and potentially treating anxiety disorders.

METHODS

Methods, including statements of data availability and any associated accession codes and references, are available in the [online version of the paper](#).

ACKNOWLEDGMENTS

We thank A. Benucci, T. McHugh, C. Yokoyama and H. Fields for comments on earlier versions of the manuscript and E. Boyden (Massachusetts Institute of Technology) and K. Deisseroth (Stanford University) for making available the optogenetic constructs used in these studies. This work was supported by funding from the Kao Corporation and Grants-in-Aid for Scientific Research on Innovative Areas (25116531, 15H01301, 16H01291), Wakate A (25710003) and Kiban B (15H04264) to J.P.J., as well as Wakate B (26830023) to T.O.

AUTHOR CONTRIBUTIONS

T.O. and J.P.J. designed the experiments and wrote up the manuscript. T.O., E.A.Y., T.A., L.-F.Y. and J.K. carried out the experiments. T.O., A.K. and J.P.J. analyzed the results.

COMPETING FINANCIAL INTERESTS

The authors declare no competing financial interests.

Reprints and permissions information is available online at <http://www.nature.com/reprints/index.html>.

- Knudsen, E.I. Supervised learning in the brain. *J. Neurosci.* **14**, 3985–3997 (1994).
- Schultz, W. Neuronal reward and decision signals: from theories to data. *Physiol. Rev.* **95**, 853–951 (2015).
- McNally, G.P., Johansen, J.P. & Blair, H.T. Placing prediction into the fear circuit. *Trends Neurosci.* **34**, 283–292 (2011).
- Ohmae, S. & Medina, J.F. Climbing fibers encode a temporal-difference prediction error during cerebellar learning in mice. *Nat. Neurosci.* **18**, 1798–1803 (2015).
- Herry, C. & Johansen, J.P. Encoding of fear learning and memory in distributed neuronal circuits. *Nat. Neurosci.* **17**, 1644–1654 (2014).
- Kim, J.J., Krupa, D.J. & Thompson, R.F. Inhibitory cerebello-olivary projections and blocking effect in classical conditioning. *Science* **279**, 570–573 (1998).
- Vallentin, D., Kosche, G., Lipkind, D. & Long, M.A. Neural circuits. Inhibition protects acquired song segments during vocal learning in zebra finches. *Science* **351**, 267–271 (2016).
- Boyden, E.S., Katoh, A. & Raymond, J.L. Cerebellum-dependent learning: the role of multiple plasticity mechanisms. *Annu. Rev. Neurosci.* **27**, 581–609 (2004).

9. Rescorla, R.A. & Wagner, A.R. A theory of Pavlovian conditioning: variations in the effectiveness of reinforcement and nonreinforcement. in *Classical Conditioning II: Current Research and Theory* (eds. Prokasy, W.F. & Black, A.H.) 64–99 (Appleton-Century-Crofts, New York, 1972).
10. Sutton, R.S. & Barto, A.G. Time-derivative models of Pavlovian reinforcement. in *Learning and Computational Neuroscience: Foundations of Adaptive Networks* (eds. Gabriel, M. & Moore, J.) 497–537 (MIT Press, Cambridge, MA, 1990).
11. Fields, H.L. & Margolis, E.B. Understanding opioid reward. *Trends Neurosci.* **38**, 217–225 (2015).
12. Fanselow, M.S. Pavlovian conditioning, negative feedback, and blocking: mechanisms that regulate association formation. *Neuron* **20**, 625–627 (1998).
13. LeDoux, J.E. Coming to terms with fear. *Proc. Natl. Acad. Sci. USA* **111**, 2871–2878 (2014).
14. LeDoux, J.E. Emotion circuits in the brain. *Annu. Rev. Neurosci.* **23**, 155–184 (2000).
15. Duvarci, S. & Pare, D. Amygdala microcircuits controlling learned fear. *Neuron* **82**, 966–980 (2014).
16. Maren, S. & Quirk, G.J. Neuronal signalling of fear memory. *Nat. Rev. Neurosci.* **5**, 844–852 (2004).
17. Tovote, P., Fadok, J.P. & Lüthi, A. Neuronal circuits for fear and anxiety. *Nat. Rev. Neurosci.* **16**, 317–331 (2015).
18. Janak, P.H. & Tye, K.M. From circuits to behaviour in the amygdala. *Nature* **517**, 284–292 (2015).
19. Johansen, J.P. *et al.* Hebbian and neuromodulatory mechanisms interact to trigger associative memory formation. *Proc. Natl. Acad. Sci. USA* **111**, E5584–E5592 (2014).
20. Johansen, J.P. *et al.* Optical activation of lateral amygdala pyramidal cells instructs associative fear learning. *Proc. Natl. Acad. Sci. USA* **107**, 12692–12697 (2010).
21. Rosenkranz, J.A. & Grace, A.A. Dopamine-mediated modulation of odour-evoked amygdala potentials during Pavlovian conditioning. *Nature* **417**, 282–287 (2002).
22. Beyeler, A. *et al.* Divergent routing of positive and negative information from the amygdala during memory retrieval. *Neuron* **90**, 348–361 (2016).
23. Annau, Z. & Kamin, L.J. The conditioned emotional response as a function of intensity of the US. *J. Comp. Physiol. Psychol.* **54**, 428–432 (1961).
24. Young, S.L. & Fanselow, M.S. Associative regulation of Pavlovian fear conditioning: unconditional stimulus intensity, incentive shifts, and latent inhibition. *J. Exp. Psychol. Anim. Behav. Process.* **18**, 400–413 (1992).
25. Johansen, J.P., Tarpley, J.W., LeDoux, J.E. & Blair, H.T. Neural substrates for expectation-modulated fear learning in the amygdala and periaqueductal gray. *Nat. Neurosci.* **13**, 979–986 (2010).
26. Belova, M.A., Paton, J.J., Morrison, S.E. & Salzman, C.D. Expectation modulates neural responses to pleasant and aversive stimuli in primate amygdala. *Neuron* **55**, 970–984 (2007).
27. Ciocchi, S. *et al.* Encoding of conditioned fear in central amygdala inhibitory circuits. *Nature* **468**, 277–282 (2010).
28. Duvarci, S., Popa, D. & Paré, D. Central amygdala activity during fear conditioning. *J. Neurosci.* **31**, 289–294 (2011).
29. Ghosh, S. & Chattarji, S. Neuronal encoding of the switch from specific to generalized fear. *Nat. Neurosci.* **18**, 112–120 (2015).
30. Fields, H.L. Pain modulation: expectation, opioid analgesia and virtual pain. *Prog. Brain Res.* **122**, 245–253 (2000).
31. Belligowan, P.S. & Helmstetter, F.J. The role of mu and kappa opioid receptors within the periaqueductal gray in the expression of conditional hypoalgesia. *Brain Res.* **791**, 83–89 (1998).
32. Gross, C.T. & Canteras, N.S. The many paths to fear. *Nat. Rev. Neurosci.* **13**, 651–658 (2012).
33. Carrive, P. The periaqueductal gray and defensive behavior: functional representation and neuronal organization. *Behav. Brain Res.* **58**, 27–47 (1993).
34. Mahn, M., Prigge, M., Ron, S., Levy, R. & Yizhar, O. Biophysical constraints of optogenetic inhibition at presynaptic terminals. *Nat. Neurosci.* **19**, 554–556 (2016).
35. Spellman, T. *et al.* Hippocampal-prefrontal input supports spatial encoding in working memory. *Nature* **522**, 309–314 (2015).
36. Di Scala, G., Mana, M.J., Jacobs, W.J. & Phillips, A.G. Evidence of Pavlovian conditioned fear following electrical stimulation of the periaqueductal grey in the rat. *Physiol. Behav.* **40**, 55–63 (1987).
37. Kim, E.J. *et al.* Dorsal periaqueductal gray-amygdala pathway conveys both innate and learned fear responses in rats. *Proc. Natl. Acad. Sci. USA* **110**, 14795–14800 (2013).
38. Han, S., Soleiman, M.T., Soden, M.E., Zweifel, L.S. & Palmiter, R.D. Elucidating an affective pain circuit that creates a threat memory. *Cell* **162**, 363–374 (2015).
39. Sato, M. *et al.* The lateral parabrachial nucleus is actively involved in the acquisition of fear memory in mice. *Mol. Brain* **8**, 22 (2015).
40. Li, H. *et al.* Experience-dependent modification of a central amygdala fear circuit. *Nat. Neurosci.* **16**, 332–339 (2013).
41. Tovote, P. *et al.* Midbrain circuits for defensive behaviour. *Nature* **534**, 206–212 (2016).
42. McNally, G.P. & Cole, S. Opioid receptors in the midbrain periaqueductal gray regulate prediction errors during pavlovian fear conditioning. *Behav. Neurosci.* **120**, 313–323 (2006).
43. Hnasko, T.S. *et al.* Cre recombinase-mediated restoration of nigrostriatal dopamine in dopamine-deficient mice reverses hypophagia and bradykinesia. *Proc. Natl. Acad. Sci. USA* **103**, 8858–8863 (2006).
44. Koutsikou, S. *et al.* The periaqueductal gray orchestrates sensory and motor circuits at multiple levels of the neuraxis. *J. Neurosci.* **35**, 14132–14147 (2015).
45. Bakal, C.W., Johnson, R.D. & Rescorla, R.A. The effect of change in US quality on the blocking effect. *Pavlov. J. Biol. Sci.* **9**, 97–103 (1974).
46. Eshel, N. *et al.* Arithmetic and local circuitry underlying dopamine prediction errors. *Nature* **525**, 243–246 (2015).
47. Tian, J. *et al.* Distributed and Mixed Information in Monosynaptic Inputs to Dopamine Neurons. *Neuron* **91**, 1374–1389 (2016).
48. Silva, B.A. *et al.* The ventromedial hypothalamus mediates predator fear memory. *Eur. J. Neurosci.* **43**, 1431–1439 (2016).
49. Reger, M.A., Gahm, G.A., Swanson, R.D. & Duma, S.J. Association between number of deployments to Iraq and mental health screening outcomes in US Army soldiers. *J. Clin. Psychiatry* **70**, 1266–1272 (2009).
50. Roy, M. *et al.* Representation of aversive prediction errors in the human periaqueductal gray. *Nat. Neurosci.* **17**, 1607–1612 (2014).

ONLINE METHODS

Subjects. Male Sprague-Dawley rats, 8 weeks old and weighing 250–275 g were singly housed on a 12-h light/dark cycle (0800/2000) and given food and water *ad libitum*. Each individual rat was housed in a single cage. All *in vivo* experiments were carried out during the light cycle. Experimental procedures were approved by the Animal Care and Use Committees of the RIKEN Brain Science Institute.

Plasmids and viral vectors. AAV5-CAG-ArchT-GFP, AAV5-CAG-GFP, AAV5-CaMKII-ChR2-eYFP, AAV5-CaMKII-eYFP and AAV5-CAG-FLEX-ArchT-GFP were produced and packaged by the University of North Carolina Vector Core. Cre-recombinase expressing canine adenovirus-2 (CAV2-Cre) was produced and packaged by Montpellier Vectorology. For trans-synaptic rabies virus experiments, glycoprotein-deleted pseudotyped EnvA-mCherry rabies viruses⁵¹ were used in conjunction with AAV2/1-ubiquitinC-Cre-recombinase (AAV2/1-Ubi-Cre) and Cre-dependent AAV2/1-FLEX-TVA, AAV2/1-FLEX-RG (rabies virus glycoprotein) and AAV5-FLEX-eYFP.

Optical fibers and single-unit recording electrodes. Single optical fibers (catalog# BFH37-200, Thorlabs) were used for behavioral experiments involving illumination of LA and for PAG illumination in conjunction with *in vivo* single-unit recording from PAG studies. The fibers were attached to lasers using a zirconia ferrule (MM-FER2007CF-2300, Precision Fiber Products). Dual fiber-optic cannulae (catalog# DFC_200/245_5.5mm_DF1.6_FLT, Doric Lenses) were used for PAG illumination during *in vivo* single-unit recordings in LA and during behavioral experiments. For *in vivo* recording experiments, the right hemisphere of either LA or PAG was implanted with a custom-made drivable microdrive containing 16 stereotrode bundles made from 0.001-inch (0.0254-mm) insulated tungsten wire (impedances ~200 kOhm; California Fine Wire Company).

Stereotaxic cannula implantation and virus/tracer injection. For all surgeries, animals were injected intraperitoneally with a mixture of ketamine (100 mg/kg) and xylazine (10 mg/kg), and supplemental doses were given as required. For behavioral experiments involving optogenetic manipulations of the CeA–PAG pathway, animals were placed in a stereotaxic frame (Leica or David Kopf Instruments) and stainless steel injection cannulae (26 gauge, Plastics One) attached to syringes (catalog #80100, Hamilton) through polyethylene tubing were targeted unilaterally (for recording experiment, right hemisphere) or bilaterally (for behavioral experiments) to the CeA (0.3 μ l/side; AP: –2.00, DV: –8.40, ML: \pm 4.30 mm). Following a 2-min preinjection period, injections were made into target sites with the flow rate (0.07 μ l/min rate) controlled by an automated pump (PHD2000, Harvard Apparatus) and this was followed by a 15-min postinjection waiting period. Following injections, bilateral optical cannulae were targeted to the dl/IPAG (AP: –7.2, DV: –4.9, ML: \pm 0.8 mm) or vIPAG (AP: –7.5, DV: –5.4, ML: \pm 0.8 mm) and affixed to the skull using stainless steel surgical screws and dental cement. For optogenetic unilateral stimulation experiments in LA, procedures were identical to those previously described²⁰. For experiments with muscimol injection into LA, surgical procedures were identical to that described above for optogenetic manipulation of the CeA–vIPAG pathway, except that following optical fiber implants in PAG, stainless steel guide cannulae (21 gauge, Plastics One) were also implanted bilaterally into LA (0.4 μ l; AP: –3.0, DV: –6.8, ML: \pm 5.4 mm). For experiments with optogenetic manipulation of RVM-projecting vIPAG neurons, CAV2-Cre (0.3 μ l) was injected to RVM (AP: –11.2, DV: –11.5, ML: \pm 0.0 mm) and AAV5-CAG-FLEX-ArchT-GFP was bilaterally injected to vIPAG (0.4 μ l/side; AP: –7.5, DV: –6.2, ML: \pm 0.8 mm). For *in vivo* recording experiments, following virus injection into CeA, custom microdrives (identical to those mentioned above) were implanted just above the LA (AP: –3.0, DV: –6.8, ML: +5.4 mm) or dl/IPAG (AP: –7.5, DV: –4.25, ML: +0.8 mm) and a ground wire was implanted into cerebellum and attached to a titanium screw. To deliver laser light into vIPAG during PAG recordings, custom-made single optical fibers (200 μ m core, NA = 0.37, identical to those mentioned above) were implanted at a 32.4° angle (AP: –7.5, DV: –5.6, ML: +1.4 mm). For LA recordings combined with optogenetic manipulation of the CeA–vIPAG pathway, dual optical fibers (described above) were implanted into vIPAG. For delivering the periorbital shock stimulus, rats were implanted with a pair of insulated stainless steel wires (0.003-inch or 0.076-mm) beneath the skin of each eyelid. For immunohistochemical experiment described below, Alexa Fluor 647-conjugated CTB (0.3 μ l) was injected into RVM (AP: –11.2, DV: –11.5,

ML: \pm 0.0 mm). For the rabies virus experiment, unilateral (right hemisphere) injections of EnvA-mCherry (0.3 μ l) were made one week after AAV cocktail injections (AAV-Ubi-Cre, AAV-FLEX-TVA, AAV-FLEX-RG and AAV-FLEX-eYFP at 1:1:1:1; 0.5 μ l in total) into the right hemisphere of vIPAG (AP: –7.5, DV: –6.2, ML: \pm 0.8 mm).

Behavioral conditioning experiment. Animals were randomly assigned to experimental groups before the start of each experiment. For all auditory fear conditioning in behavioral studies, animals were placed into a sound-isolating chamber (Med Associates) and received auditory CS (85 dB, 5-kHz tone pips at 1 Hz with 250 ms on and 750 ms off for 20 s) and electric shock US pairings. The footshock US (1-s scrambled footshock: 0.3 mA, weak shock; 0.7 mA, strong shock) was presented concurrent with the final CS pip. In the physiology experiments (see below) and a behavioral control experiment for the physiology (Supplementary Fig. 1) we used an eyelid shock US (2 ms, 2 mA (weak shock) at 7 Hz or 5 mA (strong shock) at 15 Hz for 1 s) on either left or right eyelid, beginning 300 ms after offset of final CS pip. Presentation of both CS and US were controlled by custom made software (MED-PC, Med Associates). Eyelid shocks were used for the electrophysiology experiments for better spatiotemporal shock delivery and to avoid electrical artifacts inherent in footshock. Previous studies have demonstrated the importance of the lateral amygdala in both eyelid shock and footshock induced fear learning^{14,52}, and we conducted initial control experiments comparing eyelid shock versus footshock to ensure that freezing asymptotes/aversiveness were similar (Supplementary Fig. 1 versus Supplementary Fig. 5a). For all optogenetic studies, we verified that the laser intensity was 15–20 mW from tips of optical fibers before each experiment.

For optogenetic terminal inactivation of the CeA-to-PAG projection during asymptotic learning experiments, 5–6 weeks after virus injection (AAV5-CAG-ArchT or AAV5-CAG-GFP) into CeA, dual optical cannulae were bilaterally implanted into vIPAG. After a 1–2-week recovery period, animals were alternately trained (day 1, 3) and tested (day 2, 4; 1 CS/day) twice for each (4 d in total). On training days, animals received eight CS–US (0.3 mA) pairings. Optogenetic manipulations were performed during the second training day (day 3). In the Overlap and GFP groups, orange laser (589 nm) was delivered into dlPAG or vIPAG from 400 ms before CS onset to 50 ms after US termination (total illumination time, 20.45 s). In the Offset group, laser was delivered 30–50 s (pseudorandomly) after the end of each CS–US pairing. For terminal inactivation of CeA to PAG projection during single CS–US pairing experiment, procedures were the same as above except that they only received a single CS–US (0.8 mA) pairing.

For terminal inactivation of CeA-to-vIPAG projection combined with pharmacological inactivation of LA experiments, procedures were the same as in the asymptotic learning experiment except that either PBS or muscimol was bilaterally injected (0.3 μ l, 0.25 mg ml^{–1} over a period of 60 s) into the LA 20 min before training through the chronically implanted cannulae. Injection cannulae (26 gauge, Plastics One) extended 1.4 mm from the tip of the guide cannulae (21 gauge, Plastics One).

For the optogenetic cell-body activation of LA experiment, 2–3 weeks after virus injection (AAV5-CaMKII-ChR2-eYFP or AAV5-CaMKII-eYFP) and cannulae implantation, animals were trained and tested twice using the same learning asymptote procedure described above for the CeA–vIPAG terminal inactivation experiment. However, blue laser (473 nm) was delivered unilaterally into the right LA²⁰ directly overlapping with each US during overtraining (day 3) in the Overlap and eYFP groups or 50–70 s after CS–US termination in the Offset control group.

For the optogenetic inactivation of RVM-projecting vIPAG neurons experiment, 2–3 weeks after virus injection (CAV2-Cre into RVM and AAV5-CAG-FLEX-ArchT-GFP into vIPAG) and dual optical fiber implant into vIPAG, animals were trained to learning asymptote using the procedure described above for the CeA–vIPAG terminal inactivation (days 1–4). On day 5, all rats were retrained with three CS–US pairings protocol (0.7 mA shock). On day 6, all rats received four CS presentations, during which laser illumination occurred during two of the CS (counterbalanced order). For the inactivation of RVM-projecting vIPAG cells during single-trial learning, procedures were the same as above for terminal inactivation of the CeA-to-vIPAG pathway during single-pairing experiments.

Histological verification. To verify transgene (ArchT, ChR2, CTB, GFP and eYFP) expression and the locations of optical fiber tips, cannulae and recording electrodes

in targeted brain areas, rats were killed by an overdose of 25% chloral hydrate and perfusion, and tissue sections were cut after each experiment as described previously²⁰. An experimenter blind as to animal and treatment group assessed whether transgene expression occurred specifically in the targeted brain area and whether the tips of the guide cannulae or optic fibers were dorsal and proximal to the target area or the tips of recording electrodes were below the target areas. Across all experiments, 62 animals were excluded from the analysis because these criteria were not met. After identifying the tips of recording electrodes in the tissue, we reconstructed all recording sites for each animal by calculating the distance the electrodes were advanced each day.

Freezing-response analysis. For all behavioral experiments, rats' freezing behavior during CS period was manually scored as described previously²⁰.

In vivo single-unit electrophysiological recordings in awake, behaving animals. For the electrophysiological studies, after rats had recovered from electrode implantation surgery, daily screening sessions were conducted in which electrode tips were slowly advanced (< 125 μm per d) into the targeted brain area (LA or PAG). Neurons were tested for contralateral eyelid-shock-evoked responsiveness using mild single-shock pulses (1 mA for 2 ms). If no shock responsive neurons were encountered, the electrodes were advanced.

After at least one well-isolated shock-responsive neuron was encountered in the target area, rats received auditory fear-conditioning training with 12 CS-US (2 ms, 2 mA at 7 Hz for 1 s, beginning 300 ms after offset of final CS pip) pairings presented intermittently with an average intertrial interval of 2.5 min. Following training, rats received a shock response test in which eyelid shocks were delivered under three different condition in the same context: (i) shocks delivered without preceding CS (unpredicted shock), (ii) shocks preceded by CS (predicted shock) and (iii) shocks preceded by CS combined with laser illumination into vIPAG (start 400 ms before first CS pip and end 50 ms after final shock pulse) to optogenetically inhibit CeA-vIPAG projections (predicted + laser). During these sessions, each condition was presented in a pseudorandom order eight times (24 trials in total) with the same intertrial interval as training. After that, electrodes were advanced until new cells were isolated and repeated until electrodes were no longer in the PAG or amygdala.

For both experiments, one stereotrode that did not have any isolated cells on the recording day was used as reference. Spike data were acquired through a Neuralynx data acquisition system, and spike clustering was done offline using Neuralynx SpikeSort 3D software. Principle component analyses were performed in 3D space, and spatially distinct clusters containing similar waveforms were manually identified. Single-unit isolation was further validated by ensuring that clusters remained stable throughout a recording session and that spike trains had a refractory period greater than 1 ms and mean spike amplitudes of at least 70 μV.

Electrophysiology data analysis. For all recorded neurons in LA or PAG, per-event time histograms (PETH) were constructed using timestamps of trigger events (shock or auditory tone) and spikes. The number of spikes in each bin (for a given bin size) was computed around each trigger event as

$$S_i = \frac{C_i}{N}$$

where C_i is cumulative number of spikes in the i th bin across N trials. To compare spike rates of cell populations over different distributions, S_i values were normalized to their corresponding z -scores using

$$z_i = \frac{(S_i - \mu_{BL})}{\sigma_{BL}}$$

where μ_{BL} and σ_{BL} are mean firing rate and s.d. of firing rate in baseline bins respectively. Data from PETH were used for classifying shock-US and auditory-CS responsive cells (see below).

Classification of shock-US-responsive neurons. A neuron was considered to be shock responsive during a block of trials if the 20 z_i values from bins in the 1-s shock train period of its normalized PSTH met one of two criteria: at least one bin with $z_i > 2$ or two or more consecutive bins with $z_i > 1$. All bins meeting at least one of the two response criteria in a neuron's PSTH from any trial

block (unpredicted, predicted or predicted + laser) in a shock-response test were combined. Shock-responsive cells were further classified as PE-coding or non-PE-coding cells. A frequency histogram (bin size = 0.2) of the number of shock responsive cells based on ratio

$$\beta = \frac{n_{\text{unp}} - n_{\text{pre}}}{n_{\text{unp}} + n_{\text{pre}}}$$

was plotted, where n_{unp} and n_{pre} represent the number of spikes above 99% confidence interval within the 1 s of unpredicted shock and predicted shock, respectively. Cells were categorized as PE-coding if their β score was > 0.25.

Classification of auditory-CS-responsive neurons. Cells were categorized as CS-responsive or not based on their spiking activity before and after CS onset. Baselines periods were defined as the 20-s period before CS onset in each trial. The total number of spikes during each trial in the baseline period and in the CS period was calculated, and a one-tailed paired t -test was used to categorize cells as tone activated ($P < 0.05$) or not.

Classification and analysis of freezing neurons. Freezing onset instants during intertrial intervals (20 s before unpredicted shock) were calculated using manual scoring. Freezing bouts lasting at least 1 s and equivalent nonfreezing instances during intertrial interval periods were labeled and used as Neuralynx timestamps. Spike frequency (spikes per s) around freezing onset (−50 ms to +250 ms) and during preceding nonfreezing periods were calculated and compared using one-tailed paired t -tests. Cells were classified as freezing-responsive cells if spiking frequency increased significantly during freezing onset compared with baseline values ($P < 0.05$).

Analysis of laser effects on auditory-CS and shock-US processing. For population-level analyses and to visualize the dynamics of the neural response to tones and shocks, average z_i for each cell was computed for specific cell populations (see text) within 1 s of US (bin size = 50 ms) in all three conditions (unpredicted US, predicted US without laser, predicted US + laser) and during the 20-s CS period (bin size = 250 ms) for CS alone or CS + laser conditions to generate z_i averaged PETH.

Immunocytochemistry experiment. To quantify c-Fos expression in RVM-projecting vIPAG cells, Alexa Fluor 647-conjugated CTB was injected into RVM as described above. After at least 7 d, rats were assigned into one of 3 groups: (i) a box control group, in which animals were trained by exposure to eight CS-US pairings (0.3 mA) and then exposed to a novel testing box without CS presentation on the next day; (ii) an immediate shock control group, in which animals received eight 0.3-mA shocks immediately upon entering the training box followed by eight CS presentations and were tested with five CS presentations 24 h later; and (iii) a training group, in which animals were trained by exposure to eight CS-US (0.3 mA) pairings, then tested with five CS presentations the next day. Animals were killed by perfusion 90 min after box exposure or testing on the second day. Perfusion and postfixation brain slicing procedures were identical to those described above. Brain sections (every fourth section) was then reacted with rabbit polyclonal anti-c-Fos primary antibody (1:5,000, Santa Cruz, sc-52) followed by goat anti-rabbit Alexa Fluor 594-conjugated secondary antibody (1:1,000, Invitrogen, 111-585-144). Individual Alexa Fluor 647-labeled puncta were manually counted from two vIPAG sections (of either hemisphere, counterbalanced) by an experimenter who was blinded by software (Fluoview, Olympus) to experimental group, followed by manual counting of individual c-Fos puncta. Colabeling of retrogradely Alexa Fluor 647-labeled and c-Fos⁺ cells was then calculated. To quantify c-Fos expression in RVM-projecting vIPAG cells combined with CeA-vIPAG terminal inactivation, in addition to the aforementioned CTB injection into RVM, AAV5-CAG-FLEX-ArchT was bilaterally injected into the CeA as in the behavioral experiments above. All procedures were the same as above except that in the Overlap group, orange laser (589 nm) was delivered into vIPAG during CS-US, but in the Offset group, laser was delivered during the intertrial interval period. For data analysis, the percentage (%) of Fos-IR + CTB cells was calculated by dividing the total number of Fos-IR⁺CTB⁺ double-positive cells by the total number of CTB-positive cells.

To quantify vGlut2 or GABA expression in RVM-projecting vIPAG cells, Alexa Fluor 647-conjugated CTB was injected into RVM as described above. After at

least 7 d, rats were killed by perfusion, and their brains were sectioned on a freezing microtome (for vGlut2) or vibratome (for GABA). Tissues were then reacted with rabbit polyclonal primary antibody (for anti-vGlut2, 1:200, Frontier Institute, AB_2571619; for anti-GABA, 1:5,000, Sigma-Aldrich, A2052) followed by goat anti-rabbit Alexa Fluor 488-conjugated secondary antibody (1:1,000, Invitrogen, A11034). Both Alexa Fluor 647 (CTB⁺) and 488 (vGlut2⁺ or GABA⁺) puncta were manually counted and the proportion of double-labeled CTB⁺vGlut2⁺ or CTB⁺GABA⁺ cell bodies were calculated from 3 sections/animal at rostral–caudal location matched sections. The vGlut2 antibody was selected because it labeled cell bodies (and processes) and the cell-body labeling was clearly discernible from background, particularly when identified along with CTB colabeling, which strongly labels cell bodies (see vGlut2⁺CTB⁺ and vGlut2⁻CTB⁺ examples in **Supplementary Fig. 8a**).

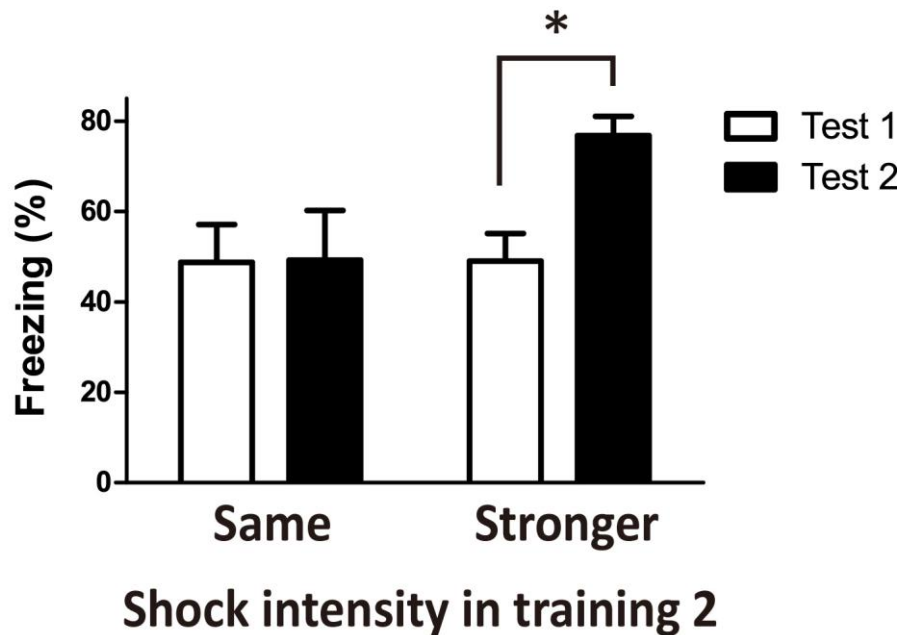
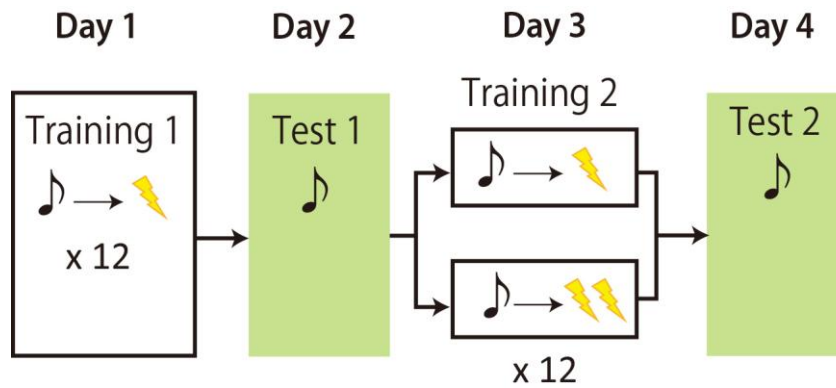
Statistical analyses. Statistical methods are shown in each figure legend for each experiment. Data distribution was assumed to be normal, and our analytic approaches were based on previously published work^{25,27,28}, but normality was not formally tested. All ANOVAs were followed by Bonferroni *post hoc* tests. For all statistical tests, significance was assessed using an α value criteria of 0.05

unless otherwise stated. All error bars show s.e.m. No statistical methods were used to predetermine sample sizes, but our sample sizes in electrophysiology, behavior and histology are similar to or larger than those reported in previous publications^{25,27,38}. For analyses, we used either Excel or Matlab scripts available through each individual software package or SPSS software package for statistical analyses.

A **Supplementary Methods Checklist** is available.

Data and code availability. The data and analysis routines that support the findings of this study are available from the corresponding author upon reasonable request.

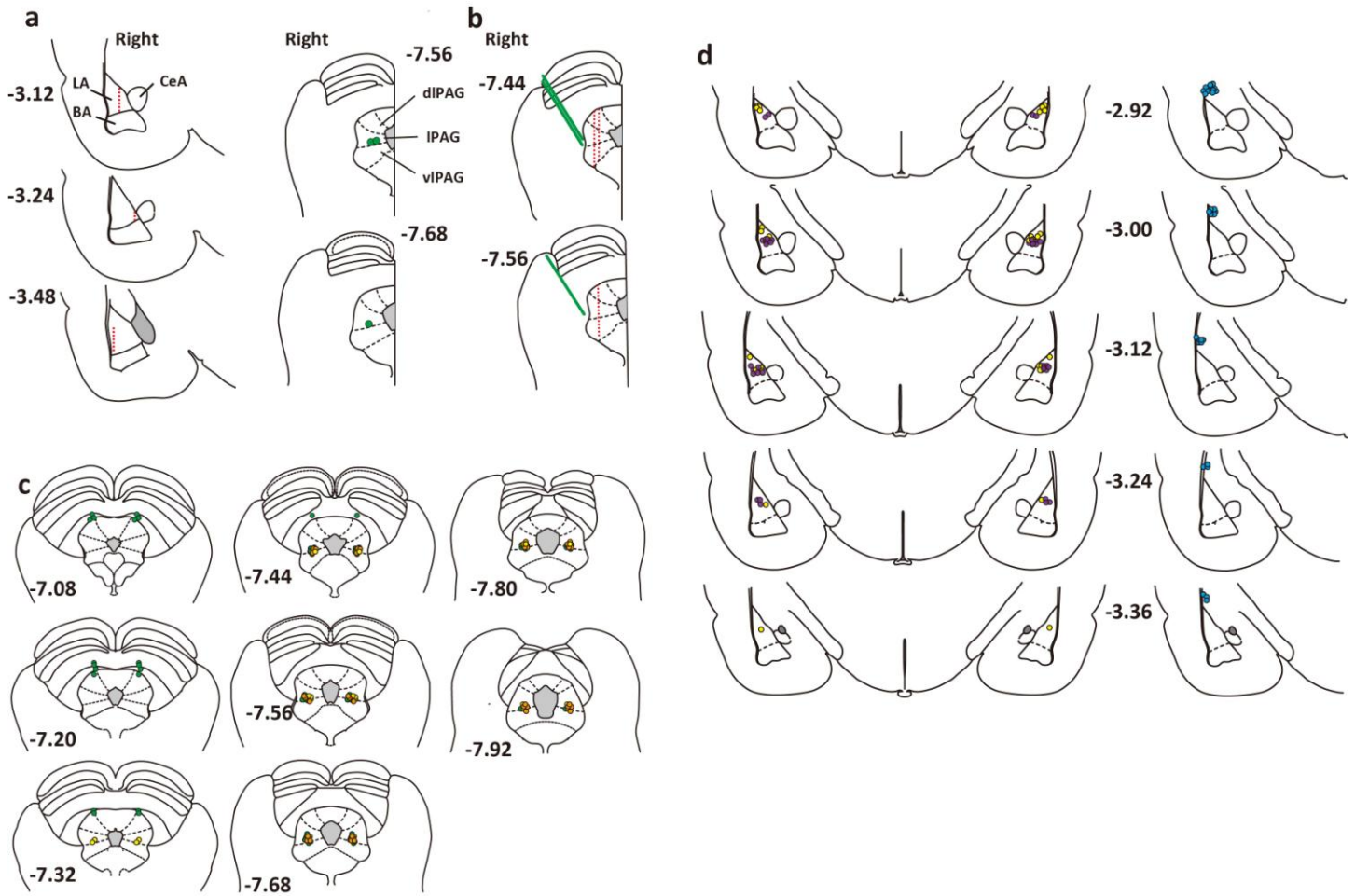
51. Callaway, E.M. & Luo, L. Monosynaptic circuit tracing with glycoprotein-deleted rabies viruses. *J. Neurosci.* **35**, 8979–8985 (2015).
52. Blair, H.T., Sotres-Bayon, F., Moita, M.A. & Ledoux, J.E. The lateral amygdala processes the value of conditioned and unconditioned aversive stimuli. *Neuroscience* **133**, 561–569 (2005).



Supplementary Figure 1

Behavioral-learning asymptote pilot study for electrophysiology studies

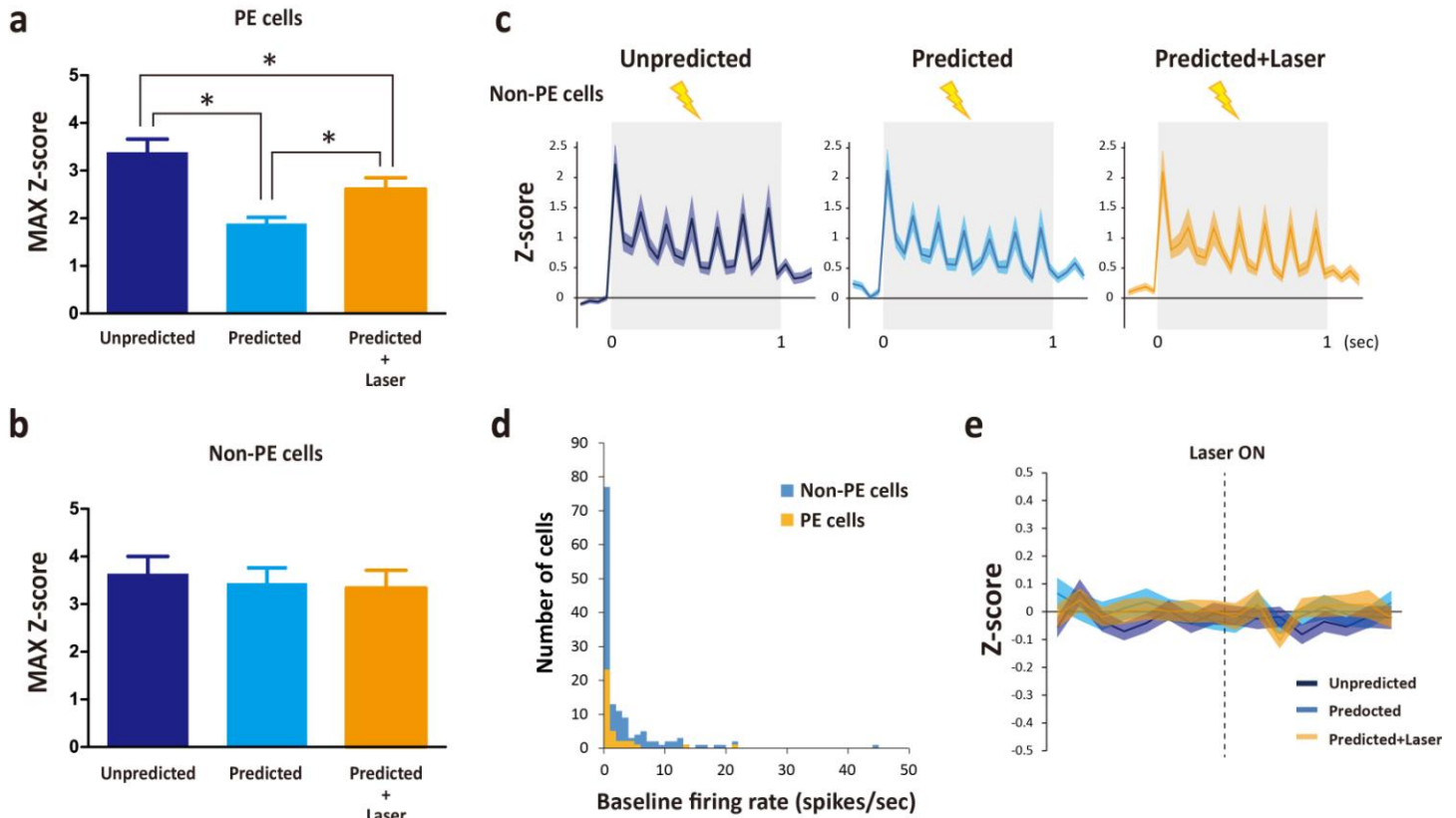
Top, Experimental design. Animals were given 12 CS-US pairings with 2mA eyelid shock intensity on Day 1, a single CS presentation on Day 2 (Test 1), 12 more CS-US pairings on Day 3 (Training 2) with some animals receiving the same shock intensity ('Same' group, n=7) and the 'Stronger' group (n=8) receiving a larger shock intensity (5mA). This was followed by another single CS presentation on Day 4 (Test 2). Bar graph (bottom) shows no change in behavioral freezing to the CS from Test 1 to Test 2 when shock intensity was the same during Training 1 and 2 ('Same' group), but an increase in CS-evoked freezing from Test 1 to 2 in the 'Stronger' group (A two-way repeated-measures ANOVA revealed significant interaction, $F_{(1,13)}=4.804$, $p=0.047$ and *post hoc* Bonferroni tests revealed no difference between test 1 and 2, $p=0.929$, in the 'Same' group, but a significant increase in freezing in the 'Stronger' group, $p=0.029$).



Supplementary Figure 2

Histological reconstruction of recording or laser illumination sites for electrophysiology and behavioral experiments

(a & b) Locations of recording sites (red dots) in LA or PAG and optical fiber (green dots or bars) in PAG during in which unpredicted and predicted shocks as well as predicted shocks concurrent with laser inactivation of CeA-vIPAG terminals were delivered. (c) Locations of optical fiber tips to deliver laser into dIPAG or vIPAG in each behavioral experiment (green dots; inactivation of terminal from CeA, yellow; inactivation of CeA terminal combined with MUS injections into LA, orange; inactivation of RVM projecting cells in vIPAG). (d) Locations of injection cannula tips to deliver drug into LA combined with (orange, in c) or without (purple) optogenetic inactivation of CeA terminal in vIPAG.

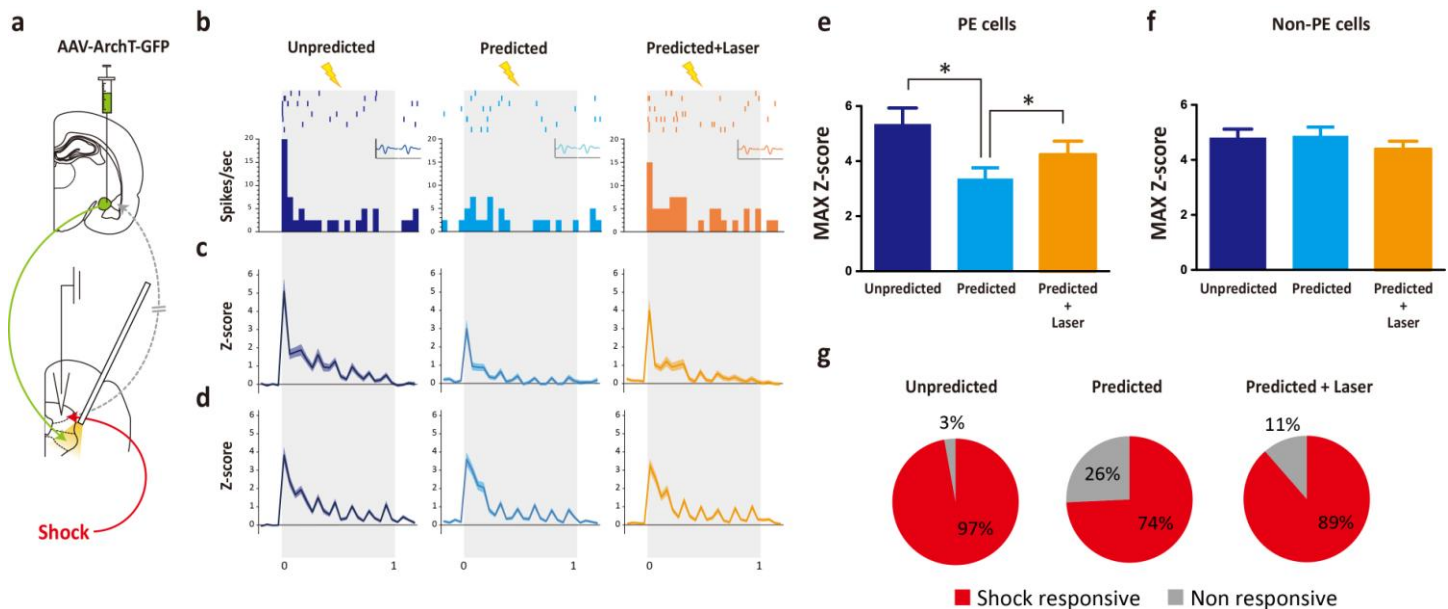


Supplementary Figure 3

Prediction-error coding in LA neurons re-emerges with optogenetic inhibition of CeA inputs to vIPAG

(a & b) Maximum Z-score averaged population response graphs with Unpredicted (navy), Predicted (blue) and Predicted+Laser (orange) bars for prediction error (PE) coding (a) or non-PE-coding (b) cell populations. For PE coding cells (a) one-way repeated measures ANOVA analysis showed a significant effect of group ($F_{(2,72)} = 16.85, p = 0.0001$). * denotes significant ($p < 0.05$) differences using Bonferroni *post hoc* tests. No change was observed in the non-PE-coding (b) cell population ($F_{(2,166)} = 1.274, p = 0.282$). (c) Perievent time histograms (50 ms bins) showing Z-score averaged responses for all LA non-PE-coding cells 'Unpredicted' (left panel), 'Predicted' (middle panel) and 'Predicted+laser' shock periods are shown in gray area (1 sec). (d) Frequency histogram showing number of total cells (y-axis) and baseline firing rates in 1 Hz bins. Blue bar heights show total cell counts and orange bar heights show total PE-coding cells in specific firing rate time bins. Based on firing rate based electrophysiological criteria established in previous work^{1,2} we found that PE coding occurs in both pyramidal (≤ 1 Hz) and fast spiking interneurons (≥ 7 Hz) replicating prior results (main ref. 25). (e) Z-score averaged perievent time histogram (bin=50 ms) for all LA neurons recorded ($n=180$) triggered by laser onset (which occurs 400 ms prior to CS onset in experiments shown in Fig. 3) for 'Unpredicted', 'Predicted' and 'Predicted+Laser' trials. Note, laser was on only in the 'Predicted+Laser' trials. No significant changes were detectable at the population level (a one-way repeated measures ANOVA, $F_{(2,166)} = 1.968, p = 0.1429$).

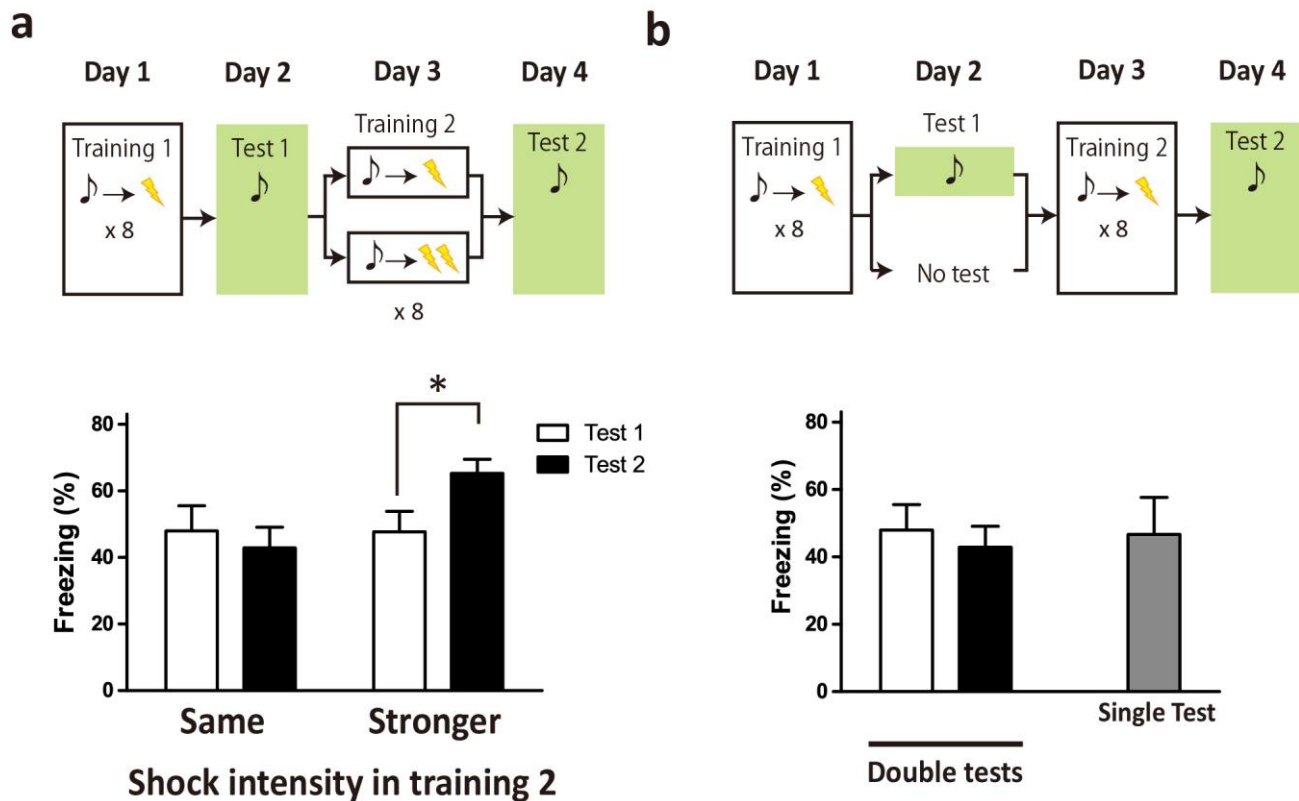
1. Likhtik, E., Pelletier, J.G., Popescu, A.T. & Pare, D. Identification of basolateral amygdala projection cells and interneurons using extracellular recordings. *J Neurophysiol* **96**, 3257-65 (2006).
2. Wolff, S.B. et al. Amygdala interneuron subtypes control fear learning through disinhibition. *Nature* **509**, 453-8 (2014).



Supplementary Figure 4

Prediction-error signaling in dl/IPAG neurons re-emerges with optogenetic inhibition of CeA inputs to vIPAG

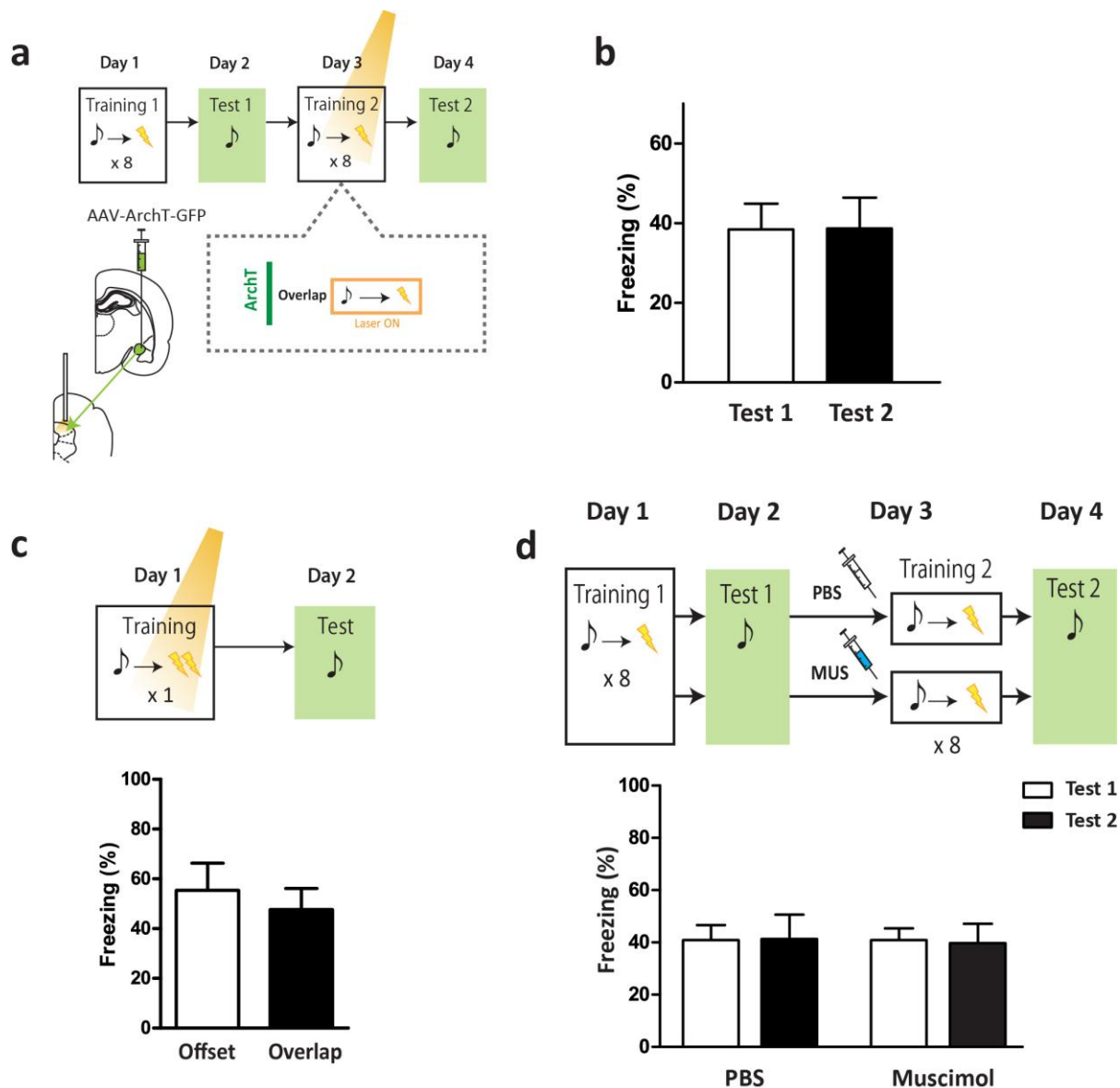
(a) Schematic of experimental paradigm showing virus injection in CeA as well as electrophysiological recording and optical stimulation sites in PAG. (b-d) Example cell and population averaged perievent time histograms (PETH, 50 ms bins) of prediction error coding cells in PAG showing disinhibition of shock-evoked responding in dl/IPAG neurons when CeA-vIPAG pathway was optically inhibited. PETHs show firing rate of an example cell (b) or Z-score averaged response (c-d) on y-axis during (gray area, 1 sec) 'Unpredicted', 'Predicted' and 'Predicted+light'. For (b), perievent raster plots are above PETHs and insets show average waveforms on two stereotrode channels during the shock period of the different trial types (total time on y-axis is 0.2 mV and on x-axis is 1 ms). PETH in (c) shows population averaged response in dl/IPAG prediction error coding neurons (n=35 out of 108 total shock responsive cells from 3 animals) with significantly (see statistics in e) larger shock-evoked response in the 'Predicted+laser' condition compared with cell responses in the 'Predicted' condition while no significant differences (see statistics in f) exist in dl/IPAG non-PE-coding neurons (d, n=73 out of 108 total shock responsive cells). (e & f) Maximum Z-score averaged population response graphs with Unpredicted (purple), Predicted (blue) and Predicted+Laser (orange) bars for prediction error (PE) coding (e) or non-PE-coding (f) dl/IPAG cell populations. For PE coding cells (e) a one-way repeated measures ANOVA analysis showed a significant group differences ($F_{(2,68)} = 13.44, p = 0.001$) and * denotes significant ($p < 0.05$) differences using Bonferroni *post hoc* tests. No change was observed in the non-PE-coding (f) cell population ($F_{(2,114)} = 2.71, p = 0.118$). (g) Circle plots showing proportion of prediction error coding dl/IPAG cells which were shock responsive or non-responsive in 'Unpredicted', 'Predicted' and 'Predicted+Laser' conditions. Chi-squared test with Bonferroni correction ($\alpha = 0.0166$) revealed a significantly higher proportion of shock responsive cells in the unpredicted vs. predicted conditions ($\chi^2_{(1)} = 7.467, p = 0.006$). There was a non-significant trend toward a higher proportion of shock responsive cells in the predicted+laser vs. predicted conditions ($\chi^2_{(1)} = 2.362, p = 0.124$), mainly because a small shock response remained in many cells resulting in a relatively large proportion of cells being classified as significantly shock responsive in the predicted condition despite their being reduced compared with the predicted condition.



Supplementary Figure 5

Establishment of a behavioral-learning asymptote paradigm to examine effects of CeA-vIPAG manipulations on behavior

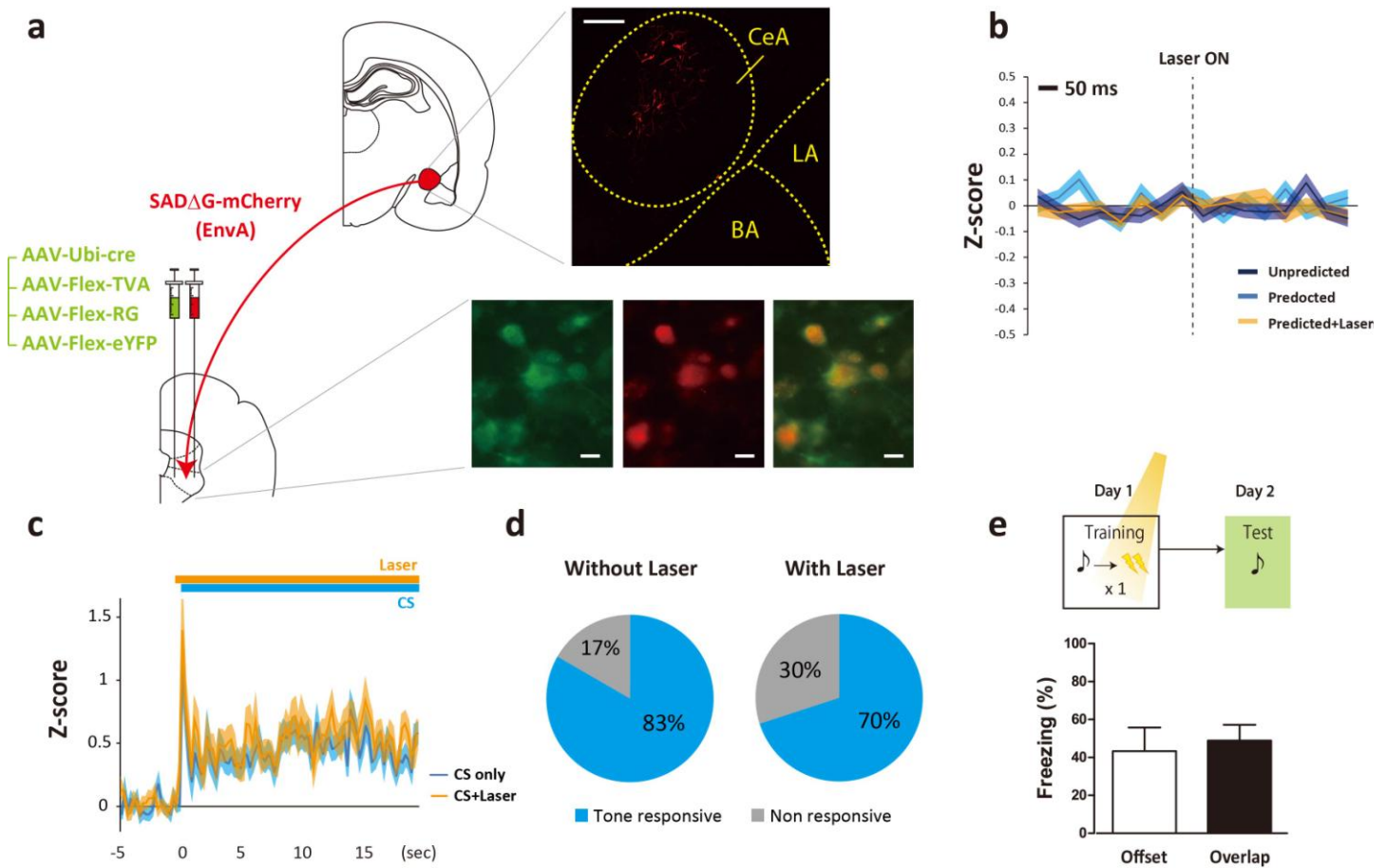
(a) Top, Experimental design. Animals are given 8 CS-US pairings with 0.3 mA foot shock intensity on Day 1, a single CS presentation on Day 2 (Test 1), 8 more CS-US pairings on Day 3 (Training 2) with some animals receiving the same shock intensity ('Same' group, n=8) and another receiving a larger shock intensity ('Stronger', 0.8 mA, n=8) followed by another single CS presentation on Day 4 (Test 2) ('Stronger' group). Bar graph (bottom) shows no change in behavioral freezing to the CS from Test 1 to Test 2 when shock intensity was the same during Training 1 and 2 ('Same' group) but a significant increase in freezing when the shock intensity was increased during Training 2 ('Stronger' group) (A two-way repeated-measures ANOVA revealed significant interaction, $F_{(1,14)} = 4.711$, $p = 0.048$, Bonferroni *post hoc* test revealed no difference between test 1 and 2, $p = 0.499$ in the 'Same' group, but a significant increase in freezing in the Stronger group, $p = 0.032$). (b) Control experiment to test whether a single CS presentation on Test 1 had an effect on learning asymptotes. Same as a, but in one group ('Single test') Test 1 was omitted and shock intensity was held constant on Training 2 (n=8 and 7, respectively). No differences were seen between Test 2 freezing (black bar) and the Single CS test 2 (grey bar) (A two-tailed unpaired t-test, $t_{(13)} = 0.3090$, $p = 0.762$) revealed that learning asymptote had been achieved after Training day 1 and the CS presentation on Test 1 had no effect on that.



Supplementary Figure 6

Offset CeA-dl/IPAG terminal inactivation, CeA-vIPAG terminal inactivation effects on single-trial learning and muscimol effects on learning asymptotes

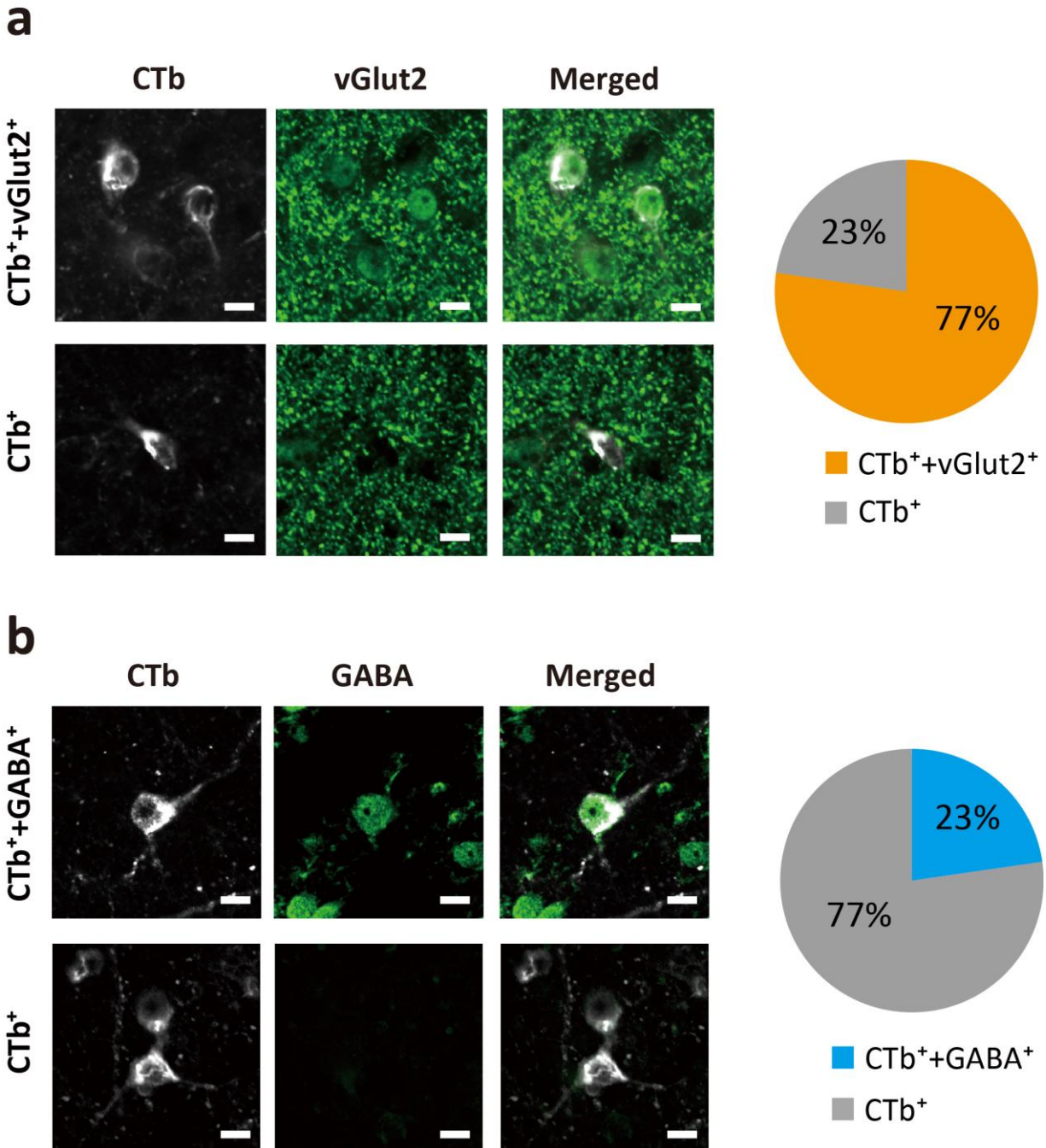
(a) Schematic of experimental paradigm showing optogenetic manipulation of CeA-dl/IPAG pathway specifically during overtraining/learning asymptote. (b) Inhibition of CeA-dl/IPAG pathway during auditory CS and shock US periods of overtraining ($n=10$) does not change freezing levels (y-axis) from Test 1 compared with Test 2 (Two-tailed paired t-test, $t_{(9)} = 0.041$, $p=0.9682$) (c) Top, Schematic of experimental paradigm showing optogenetic inhibition of CeA-vIPAG pathway during auditory CS and strong shock US (0.8mA) periods of single trial (1 CS-US pairing) fear conditioning. Bottom, inhibition of CeA-vIPAG pathway has no effect on single trial learning as measured 24 hours following learning and optogenetic manipulation comparing 'Offset' to 'Overlap' group ($n=7$ and $n=7$ respectively) (Two-tailed paired t-test, $t_{(12)}=0.5571$, $p=0.588$). (d) Muscimol alone in LA has no effect on learning asymptotes. Top, Experimental design. Animals are given 8 CS-US pairings with 0.3 mA foot shock intensity on Day 1, a single CS presentation on Day 2, 8 more CS-US pairings on Day 3 (Test 1) at the same shock intensity and 1 more CS presentation on Day 4 (Test 2). Prior to Training 2 animals received microinjections of phosphate buffered saline (PBS) as a control or the GABAA agonist Muscimol to inactivate LA neurons. Bar graph (bottom) shows no change (Two-way repeated measures ANOVA, $F_{(1,14)}=0.0567$, $p=0.815$) in behavioral freezing to the CS from Test 1 (white bar) to Test 2 (black bar) in PBS and Muscimol treated animals.



Supplementary Figure 7

CeA-vIPAG trans-synaptic rabies virus tracing, effect of CeA-vIPAG inactivation on auditory responding in dl/IPAG cells and baseline firing rates in PAG neurons, and effect of inactivation of RVM-projecting vIPAG neurons on single-trial fear learning

(a) Schematic showing injection of rabies virus (SADΔG-mCherry) along with 3 different cre-dependent (FLEX) AAVs expressing TVA, glycoprotein (RG), eYFP and a ubiquitously expressed AAV-cre-recombinase. *Bottom right inset* shows starter cells in vIPAG coexpressing mCherry (red) and eYFP (green) and the overlay. Scale bar=10 μm. *Top right inset* showing retrogradely labeled, rabies virus infected mCherry expressing cells in CeA. Scale bar=200 μm (b) Z-score averaged perievent time histograms (bin size=50 ms) for vIPAG neurons (n=147) triggered by laser onset (which occurs 400 ms prior to CS onset in experiments shown in Fig. 1 & 2) for 'Unpredicted', 'Predicted' and 'Predicted+Laser' trials. Note, laser was on only in the 'Predicted+Laser' trials. No significant changes were detected (One-way repeated measures ANOVA, $F_{(2,292)}=0.557$, $p=0.574$). (c) PETH showing population averaged firing rates (y-axis) of all CS-responsive cells in dl/IPAG (n=50 out of 113 total cells) during the auditory CS period (20 sec starting at '0', x-axis) without (blue trace) or with (orange trace) light induced inhibition of CeA-vIPAG pathway. Auditory CS (blue bar) and laser on (orange bar) periods are denoted above PETH. A two-tailed paired t-test revealed no effect of terminal inhibition on CS-evoked excitatory response in LA ($t_{(64)}=0.0508$, $p=0.96$). (d) Circle plots showing proportion of dl/IPAG cells which were significantly auditory CS-responsive (blue) or non-responsive (grey) with and without laser inactivation of the CeA-vIPAG pathway. Chi-squared test revealed no significant difference in the proportion of CS-responsive cells between with and without laser conditions ($\chi^2_{(1)}=2.918$, $p=0.0876$) (e) *Top*, Schematic of experimental paradigm showing optogenetic inhibition of RVM projecting vIPAG neurons during auditory CS and strong shock US (0.8 mA) periods of single trial (1 CS-US pairing) fear conditioning. *Bottom*, inhibition of RVM projecting vIPAG neurons had no effect on single trial learning as measured 24 hours following learning and optogenetic manipulation comparing 'Offset' to 'Overlap' group (n=8 and n=8 respectively) (Two-tailed paired t-test, $t_{(14)}=0.3728$, $p=0.715$).



Supplementary Figure 8

RVM-projecting vIPAG neurons are mostly glutamatergic while a smaller subpopulation is GABAergic

Retrograde tracer (CTb Alexa 647) injections were made into the RVM and tissues were immunostained for vesicular glutamate transporter-2 (vGlut2) or GABA. **(a)** Top images ('CTb+vGlut2+') show examples of vGlut2⁺ cells colabeled by CTb. Note vGlut2 fiber label labeling along with clear soma labeling. Bottom 'CTb+' images show CTb labeled cell without vGlut2 cell body labeling. Pie-chart shows proportion of double labeled cells (vGlut2+/CTb+) in all CTb⁺ cells counted (n=528, from 3 animals). **(b)** Top images ('CTb+/GABA+') show examples of GABA⁺ colabeled by CTb⁺. Bottom 'CTb' images show CTb labeled cells without GABA labeling. Pie-chart shows proportion of double labeled cells (GABA+/CTb+) in all CTb⁺ cells counted (n=1575, from 3 animals). Scale bar=10µm.